PbTe nanocrystal synthesis, chemical passivation and self-assembly into atomically coherent superstructures via oriented attachment

Marc Smits

Supervisors:

Carlo van Overbeek

Daniël Vanmaekelbergh

Master thesis

30-9-2016

Abstract

Using oriented attachment two dimensional superstructures of PbTe quantum dots were synthesized. PbTe nanoparticles in the range of 4-5 nm were synthesized using the hot injection method. Due to the low stability of PbTe under ambient conditions the nanoparticles were treated using halogens. The higher stability under ambient condition makes them easier to use in future applications. This treatment helps in reducing the speed at which the particles oxidize and Bromide protects the particles against oxidation the best. The halogen treatment doesn't hinder the particles during oriented attachment and appear to help synthesize larger structures due to the increased stability. Different superstructures were synthesized, ranging from honeycomb to linear and square structures. Square superstructures with patch sizes of about 200 nanometres can be synthesized with about 60% reproducibility. The square structures can be synthesized fairly reproducible but aren't guaranteed, therefore increasing the reproducibility further could make further analysis of the structures, for example the electronic structure with STM, easier.

Contents

Introduction

When graphene was discovered they found it had a very high electron mobility. This mobility is not only due to the material but also the honeycomb structure [1]. Making structures with other material containing the same honeycomb structure or very similar lattice became an interesting and challenging next step. Other materials with the same honeycomb structure might also show high electron mobility.

Graphene doesn't have a band gap, nanocrystal of the lead chalcogenide family have a band gap in the infrared and experiments have shown these nanocrystal can form multiple superlattices [2] [3]. One of these superlattices is a honeycomb lattice which is slightly buckled [2] [4].

These superlattices are made using an oriented attachment method as described in literature [3]. Using this method the nanocrystal fuse together and make one large crystal. This has an advantage over self-assembly method because there is no more barrier, ligands, between the particles. In a self-assembly this barrier between the particles lowers the conductivity significantly, to lower this barrier the ligands are exchanged for shorter ligands [5]. Another advantage of this method is that these superlattices can be deposited on many different substrates.

The material used in this thesis are PbTe nanoparticles. PbTe has a high spin orbit coupling which might be interesting for future application in computer chips. These nanoparticles are synthesized using a hot-injection method. Due to PbTe being very sensitive to oxidation by oxygen the particles are treated with halogens. For the other lead chalcogenides this treatment increased the stability under ambient conditions considerably [6] [7]. Next superlattices were synthesized using the method similar to the experiments in literature [2] [3]. In these papers PbSe is used and in order to get more insight into the formation mechanism it’s interesting to know if it is also possible to make these structures using a different but similar material.

Some theory will be discussed to better understand the procedures and results obtained. First about quantum confinement, the synthesis of nanocrystals, self-assembly and oriented attachment. Next the experimental method will be explained and the measurement equipment that has been used. Afterwards the results are discussed and finally the conclusions and an outlook for future research.

Theory

Nanocrystals are nanoparticles with dimensions of 2 to 100 nm in size [8]. When all the dimensions of a semiconductor nanocrystal are smaller than the exciton Bohr radius of the material it's often called a quantum dot. The exciton Bohr radius is the (approximate) size of a hole-electron pair. This radius is important for nanoparticles, because when one of the dimensions of a semiconductor nanocrystal become smaller then this radius quantum confinement effect start to appear [9]. These confinement effects appear because the electron-hole pair becomes physically confined in the nanocrystal. These effect have an influence on the optical and electronic properties of the particles. One of the most known and studied effect is the size dependency of the optical emission. This effect increases the bandgap of the material when the confinement energy increases. This will be explained further in the quantum confinement part of the theory. Other topics discussed in the theory section are the synthesis of nanocrystals, self-assembly and oriented attachment. The first two parts are summarized from the book of C. de Mello Donegá [10], if you are interested in more details about quantum confinement or synthesis of nanoparticles I would like to refer you to read this book.

Quantum confinement

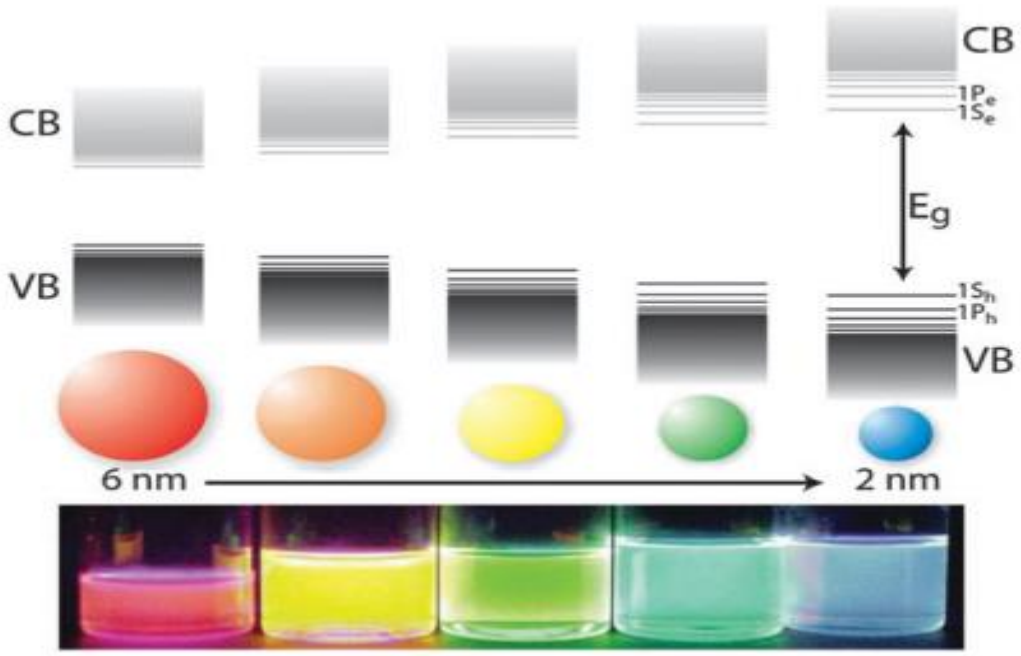

Figure 1. On the bottom of the picture the quantum confinement effect is shown for CdSe quantum dots [8]. On the top it shows the evolution of the electronic structure from large nanocrystal (left) to small nanocrystal (right).

Figure 1 shows the quantum confinement effect. There are two effects that are visible due to quantum confinement: increase of the bandgap of the material and the appearance of discrete energy levels at the band edges. These effects can be explained using two approaches: top-down approach and the bottom-up approach. The bottom-up approach will be explained below.

In Figure 1 the quantum confinement effect is shown for CdSe quantum dots, it shows the tunability of the emission by changing the size of the quantum dots and therefore the band gap [8]. This increase in band gap is also visible in the absorption wavelength, this also shifts to higher energies for smaller quantum dots. Another thing that is visible in the absorption spectrum is the appearance of multiple peaks at higher energies [5]. These extra peaks are due to the discrete energy levels at the valence and conduction bands. In the strong quantum confinement regime the energy difference between the energy levels is of the order of a couple of hundreds of meV. This is enough energy difference for the levels to be visualized in the spectrum.

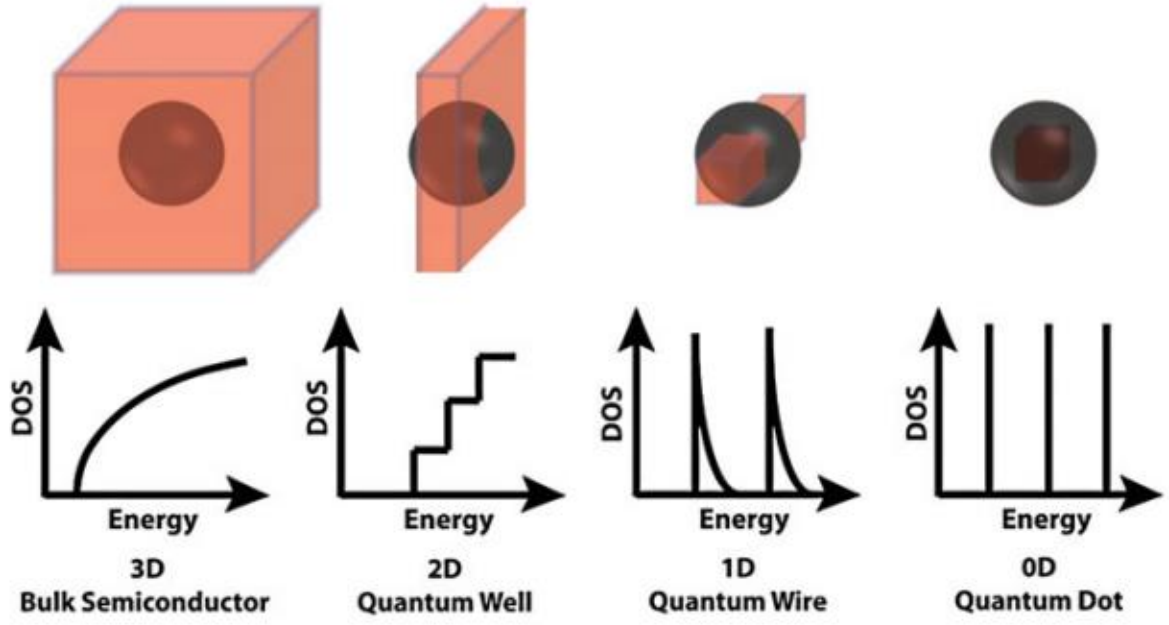

Figure 2. Schematic representation of the energy levels of different nanostructures. The most left structure is from the bulk and the circle represent the exciton Bohr radius of the material [9].

Above we only talked about quantum dots, a structure where the exciton is confined in all directions. This is an example of a zero-dimensional structure, but also a lot of other structure can be made. With 1 dimensional structures you can think of nano rods or nanowires and 2 dimensional structure for example platelets or disks. These structure continue to show discreet energy levels when at least one of the diameters is less than a_0. If this is the case for a nano rod or wire the structure can also be called a quantum rod or wire, the length of a wire is many times a_0 while in a rod it's only a couple of times a_0 long. If there is only quantum confinement in 1 direction the material is called a quantum well. The energy level structure of the nanostructures are shown in Figure 2**.**

Bottom up approach

In this approach the nanostructure is considered a very big artificial atom. We start from one atom and make it bigger by adding more and more atoms. This is done by using LCAO (Linear Combination of Atomic Orbitals), the wave function of the quantum dot is constructing from many individual atomic orbitals.

To explain this method we first look at a simple molecule with multiple electrons, a hydrogen molecule. In the molecule two hydrogen atomic orbitals (AO) are combined to form two molecular

orbitals (MO). These two molecular orbitals are spread out over the hydrogen atoms into one bonding orbital, lower in energy, and one anti-bonding orbital, higher in energy. Both hydrogen atoms have one electron and both of these electrons combine into an electron pair in the bonding orbital. If for example there were more than two electrons one will be in an anti-bonding orbital and weaken the bond between the two hydrogen atoms. The orbitals are filled in a way the energy is minimized. The highest filled orbital is called the HOMO (highest occupied molecular orbital) and the lowest unfilled orbital is called the LUMO (Lowest unoccupied molecular orbital).

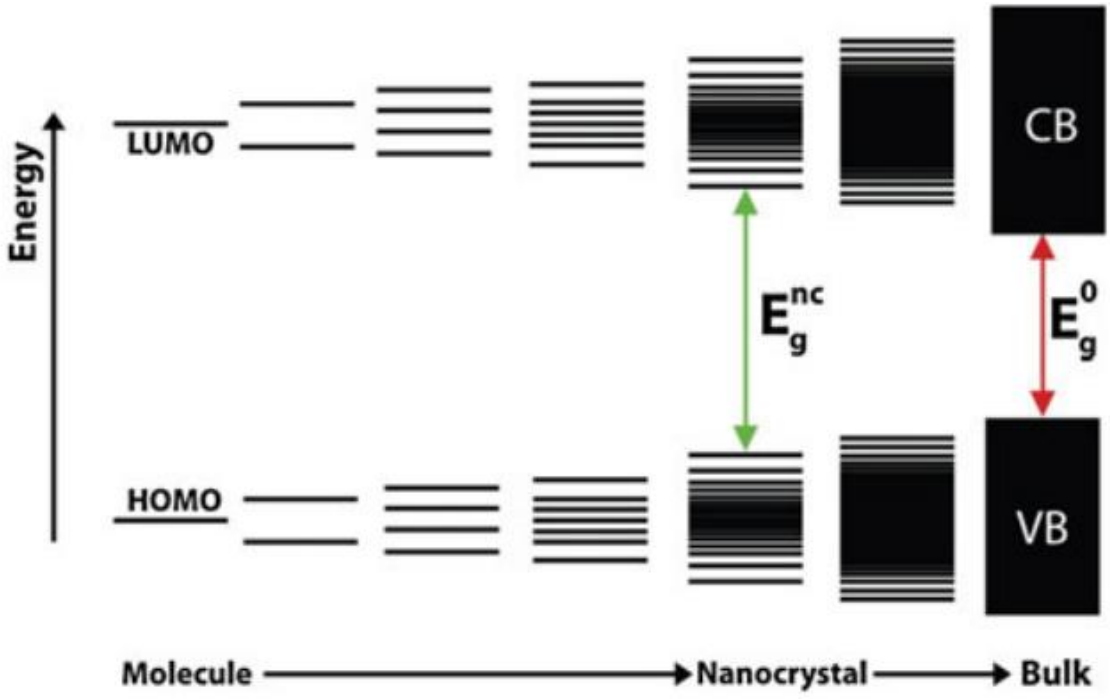

Figure 3. Formation of energy levels for semiconductor material, on the complete left a hypothetical diatomic molecule and on the right a bulk semiconductor. The band gaps are shown by $E_g^{Nc\ or\ 0}$ and indicate the energy difference between the HOMO and LUMO or VB and CB respectively [11].

This method can also be used for a quantum dot, consisting of many atoms. We start from one 'molecule', for example PbTe, which gives one AO for both Pb and Te and combine to two MO like in the hydrogen molecule, an antibonding orbital and a bonding orbital. Now we start adding more molecules, this leads to multiple AO and therefore more MO. The molecular orbitals will all have slightly different energies than the first two. After adding more a trend becomes visible, around the first MO's the density of levels is higher than at the edges, also the distance between the highest bonding orbital and the lowest anti-bonding orbital gets smaller. If we continue adding molecules we get closer to the bulk crystal, at this moment there are so many MO and the spacing between each of the bonding and anti-bonding becomes so small, we can consider them both like quasi-bands. The quasi-band formed by the bonding orbitals is analogues to the conduction band and the anti-bonding states to the valence band. With this simple model the above stated effects can be explained, separated energy at the edge of the valence and conduction band and the increase in bandgap with decreasing size. This is schematically shown in Figure 3.

Quantum dot synthesis

Nanocrystals can be made using a variety of ways some example are: by injecting precursors in a solvent at high temperature or from a bulk crystal by removing material from the top and sides. These methods are similar to the two approaches described above where the synthesis from solution is a bottom up approach and the synthesis from bulk a top down approach. An example of going from bulk to a nanocrystal is by use of lithography, here material is burned away from the top and sides of a piece of bulk material to from a nanocrystal. This method is heavily used in the computer chip industry to make the chips which are used for examples in computers or phones [10].

Two examples of bottom-up synthesis methods are molecular beam epitaxy (MBE) or colloidal synthesis. In MBE the material precursor are introduced in the gas phase and deposited on a substrate. This method allows to grow atomic layers of different materials on top of each other to synthesize different confined nanostructures. A disadvantage of this method is the cost to make these structures. The colloidal synthesis take place in a solution and allows easier post synthesis treatments. The cost are lower and scalability of this method is also bigger and this method allows easier access to particles in the strong confinement regime as the beam in MBE has a definite size and is limiting the final size of the nanoparticles [8]. As the colloidal synthesis method is also used in this thesis we will have a closer look to this method.

As stated above the colloidal synthesis is performed in a solution. To keep the nanoparticles stable they are coated with a layer of surfactant molecules, ligands. In most synthesis long chained fatty acids or amines are used, for example oleic acid or oleylamine [5] [8] [12]. These ligands give the particles stability in the solvent, preventing them from dissolving and oriented attachment aggregation. Most ligand have a polar head group, most containing an oxygen, sulphur or phosphine, and an organic tail. The surfactants on the surface of the nanoparticle can also be an ion or inorganic molecule. The tail determines mostly the interaction with the solvent and therefore the length and functional group determine if the particles stay in solution or precipitate. The ligand tails also prevent colloidal aggregation of the nanoparticles by repulsive van der Waals and electrostatic interactions [8].

The strength with whom the ligands bind to the nanoparticles is determined by the nature of the head group and also the length of the ligand tail length. The strength with which the ligands bind to the nanoparticles determines their stability, but also the growth rate during synthesis. Choosing the right kind of ligands for your goal, this is especially important for post synthesis procedures like cation exchange or embedding in silica. For both of these processes fast exchanging ligands [8]

The head group (amines, oxygen, sulphur or phosphine) can be put into groups of hard and soft Lewis bases. Oxygen is for example a hard Lewis base due to its small size and large electronegativity, sulphur on the other is a soft base. The Lewis acids are the metal atoms, hard acids are small highly charged metals like zinc and soft acid metals are for instance lead.

The phosphines ligands however prefer binding to the chalcogenides or transition metals. The phosphines form sigma donating and pi back donating bond with the metal. The binding strength is also depending on the type of groups attached to the phosphine, monodentate < bidentate < tridentate, where tridentate ligands (three bonds to the phosphine) make the strongest bonds

between phosphine and the nanoparticle. The chain length of the ligands is also important to keep in mind, longer chain keep the particles further apart, but on the other hand also more bulky and might inhibit sufficient particle coverage. Short chained ligands binds less strongly to the surface and are therefore more dynamic and also allow shorter particle particles distances [8] [5].

The ligands are not solid on the nanoparticle surface but can move [8], bundle or form denser and open assemblies [13]. This movement of the ligands can be important in the formation of nanoparticles self-assemblies. They prevent the particles of getting to close to each and by controlling the assemblies of the ligands different places are more accessible. The ligands also influence the optical properties. The ligands passivate dangling bonds which are trap states for the emission, these dangling bond states lay close to the HOMO and LUMO states, by passivation them they shift the energy away. Some ligands are also able to take away the charge carriers from the nanoparticles and therefore also quench the luminescence.

As stated above ligands are not solid, but still mobile on the surface of the nanoparticles. Ligands can also be exchanged for different ligands [5] [6], this is sometimes useful for further synthesis steps or changing the solvent. Depending on the type of ligand the ligand exchange can be performed directly after synthesis without purification [6], for stronger binding ligands, or only after purifications for weaker binding ligands. For weaker binding ligands an excess of the new ligands is required to exchange most of the ligands. The binding strength is also facet dependent, meaning that high energy facets bind ligands stronger than lower energy facets. High energy facets are crystal planes which have a high surface energy due to many dangling bond. Amphiphilic ligands can also be exchanged with halogens or inorganic molecules in a similar way [6].

Colloidal synthesis

First we start with a brief summary of theory and equations about the colloidal synthesis. The colloidal synthesis can be divided in three different stages: induction, nucleation and growth. All these steps and the evolution of the supersaturation is shown in Figure 4. The first step, the induction, is the formation of the elemental monomers (K_1). These monomers starts to form “sub-critical nuclei” (K_2), unstable clusters of multiple monomers.

The formation speed of monomers depends on the type of precursors used in the synthesis. The chalcogenides dissociate faster from the phosphine the bigger the atom gets. The hard/soft Lewis acid/base rules also apply here, hard Lewis acid bind stronger to hard Lewis bases. Here also stronger bonds leads to slower dissociation speed.

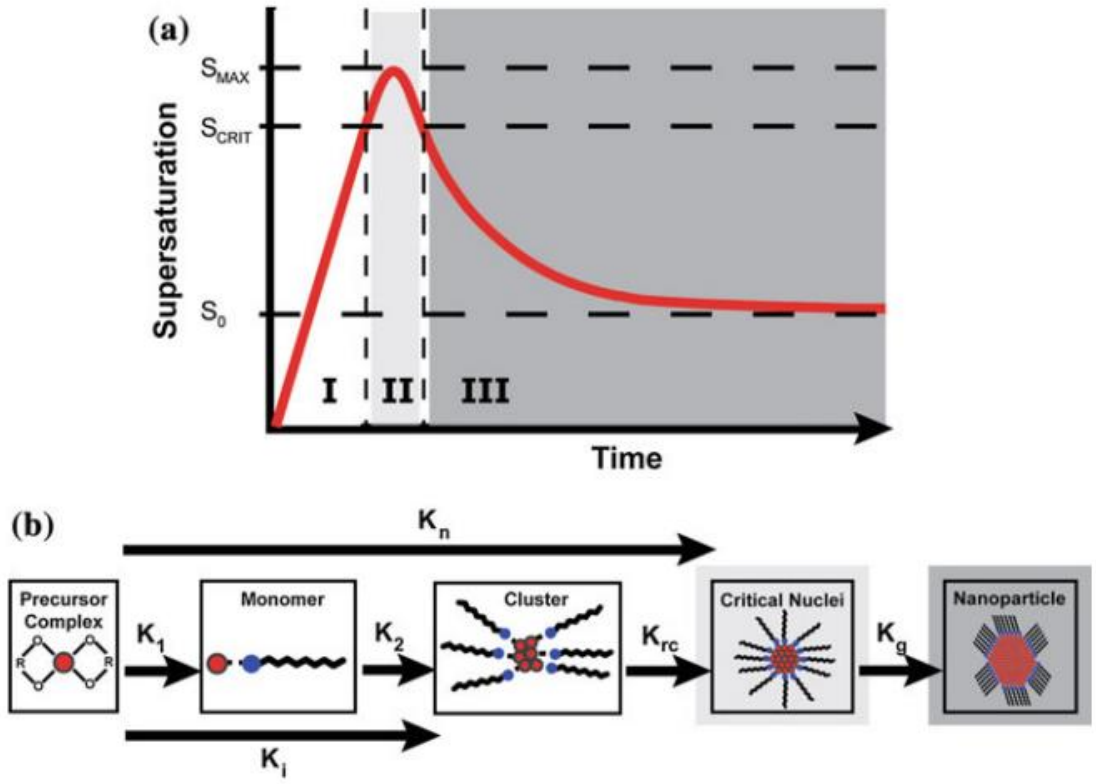

Figure 4. In part (a) of the figure the evolution of the supersaturation is shown as a function of time. Part I is the induction of the nanoparticle synthesis: formation of monomers and clusters. Part II is the formation of critical nuclei, the large amount of critical nuclei formed lead to a decrease in supersaturation. Part III is the growth of the nanoparticle further decreasing the supersaturation. Part (b) is a visible representation of each step in the synthesis with the names of the different rate constants [10].

In the second step, nucleation, the cluster grow bigger and grow above the critical radius (r_C). At this radius the chance that the particles grow or dissolve is equal. The rate constant for the formation of these critical nuclei is k_{rc}. The formation of critical nuclei takes place by addition of monomers or the coalescence, the agglomeration of 2 or more clusters into one. The effective nucleation will be equal to the slowest rate, k_{rc} or k_i.

Nuclei form due to the monomer supersaturation, the concentration is higher than a critical value (S_{crit}). The oversaturation is equal to the ratio between the solute activity in the reaction and the solute solubility. This oversaturation is unstable, because the amount of monomers is larger than the solubility limit. The oversaturation rate is maintained as long as the rate k1 is larger than the rate at which monomers are consumed.
The nucleation can be modelled using the classical nucleation theory [8]. We use the model only to discuss the principle involved and not the model itself. One of the requirements for nucleation is an oversaturation, formed by a sudden injection of monomers or a change in the solubility. The driving force is the free energy difference between monomers in the crystal phase and the monomers in solution. The total free energy change (ΔG_{TOT}) for the nuclei is given by [10]:

$$\Delta G_{TOT} = \Delta G_V + \Delta G_S = \frac{4}{3}\pi r^3 \rho \Delta\mu + 4\pi r^2 \gamma$$

In this formula ΔG_V and ΔG_S are the volume or surface free energy. The volume free energy is negative because of the released energy by the formation of bonds in the nucleus. The surface free energy is positive because of the high amount of dangling bonds at the nucleus. P (rho) is the crystal density and Δμ is the chemical potential difference between nucleus and solvent. This value can be approximated using –kTlnS. As described above S is the oversaturation and can also be written as $S=a/a_0$. At a given temperature T a is the monomer activity in the reaction mixture and a_0 is the solubility limit. In a multicomponent material, a will be determined by the product of both components in the reaction solution ($a=a_M a_E$). a_0 is the solubility product constant K_{sp} at T. γ is the interfacial tension between nucleus and solution. The formula will reach a maximum value at the critical radius r_C, this results in nuclei dissolving again when there size is $r<r_C$, while nuclei $r>r_C$ continue growing as long as there are monomers. The critical nucleus radius can be calculated using [8] [10]:

$$r_c = -\frac{2y}{\rho kTlnS}$$

This formula shows that the critical radius becomes smaller with increasing temperature and oversaturation. A supersaturation of a minimum value S_{Crit} is required, otherwise the chance for the formation of a nucleus is too small.

In the last step the nuclei start to grow larger by monomer addition, coalescence or both. The rate of the growth is k_g, this is an averaged rate. In practice most reactions are stopped before the growth of the particles has stopped. This is due to a side reaction called Oswald ripening. During Oswald ripening smaller particles stop growing or start shrinking, on the other hand larger particles continue growing. The reason the small particles stop growing or shrink is due to the difference in surface energy, small particles are more reactive and less stable then large particle. This increases the size distribution and this is unfavourable in most synthesize.

The growth can be explained using two main routes: coalescence and monomer growth. With coalescence the particles or nuclei grow by one particle agglomerating with another particle. Next the particle goes through a reconstruction to form a new larger particle. This process might play a key role in the formation of anisotropic shaped particles like nanowires and nanorods. When this process happens in a facet specific place the process is also called oriented attachment. This process will be later explained in more detail.

The growth via addition of monomers has two important steps: diffusion to the particle and incorporation into the particle. The opposite processes also take place, but only when the monomer concentration is low (Oswald ripening). The growth rate can be expressed using [10]:

$$\frac{dr}{dt} = \frac{DV_m(a_b - a_r)}{r - (\frac{D}{K_s})}$$

In this formula D is the monomer diffusion coefficient, V_m the molar volume of the solid, a_b the monomer activity (far from the NC), a_r is the NP surface activity (similar to the NP solubility) and K_s the reaction constant between monomer and NP surface. The activity is used because the behaviour is not ideal. The driving force for diffusion is the concentration gradient between the NP surface and the solvent. The monomer activity and diffusion coefficient in the reaction medium, which is a

function of the temperature and the growth solution composition. The diffusion can be increased by increasing the temperature, the monomer concentration and decreasing the amount of surfactants in the solution.

During the synthesis there are two growth regimes: the reaction controlled regime and the diffusion controlled regimes. The reaction controlled regime holds at high monomer activities (concentration), here the diffusion is so fast that it can be neglected. The first growth is therefore considered to be reaction controlled. When the monomers in the direct environment around the particles is depleted will the diffusion be the limiting step. At this moment the monomer activity in the solution is low and the dissolution rates of the particles increases and becomes comparable to the deposition rate. This is the regime where Ostwald ripening occurs.

The dissolution rates are size sensitive, this is due to the Gibbs-Thomson relation. This relation states that spherical particles with radius r have extra chemical potential and this increases the solubility for small particles compare to large particles. The activity at size r can be approximated using [10]:

$$a_r = a_0 \exp\left(\frac{2\gamma V_m}{r k_B T}\right)$$

a_0 is the monomer activity in equilibrium with bulk and k_B is the Boltzmann constant. The exponential term is much bigger for the nanoparticles then for bulk due to the large difference in interfacial tension at the nanoscale. The critical size r^* which is in equilibrium with the solution can also be defined using the Gibbs-Thomson relation. This allows us to write the growth rate as a function of this critical size [10]:

$$\frac{dr}{dt} = \frac{2\gamma D a_0 V_m^2}{k_B T r}\left(\frac{1}{r^*} - \frac{1}{r}\right)$$

The size r^* is comparable with the r_C (critical nucleation size), particle sizes smaller than r^* will shrink, while particles larger than r^* will grow. This equation tells us that the monomer activity determines the size distribution during the growth. At high monomer activity the size distribution will get smaller, this will be called size distribution focusing (reaction controlled regime). At high monomer activity all particles will grow, but due to the difference in surface area smaller particles will grow faster and big particles will grow slower.

At lower monomer concentration the r^* will increase and smaller particles start to dissolve faster due to their higher surface/volume ratio and higher surface energy. Now the process of Ostwald ripening starts to take place and the size distribution becomes bigger.

Self-assembly

Self-assembly is the spontaneous arrangement of sub mm particles into ordered structures [3] [14] [15] [16]. This self-assembly happens by interactions of the surface of the particles with neighbouring particles either entropic driven or energy driven [17]. Purely entropic driven self-assembly form from non-interacting particles and can be described using a hard sphere model [17].

Most synthesized particles do have interactions with each other, by charged ligands or surfaces, magnetic interactions or activated facets [15] [16] [17]. This interactions leads to the formation of structures were the total free energy is minimized by aligning magnetic fields or charges [16]. The systems in which self-assembly happens don't have to be consisting of only one type of particles but also binary system can form self-assembly into ordered superlattices [17].

Self-assemblies form from evaporating the solvents in which the particles are suspended onto a substrate [17]. By the evaporation of the solvent the particles lose their three-dimensional freedom and have less space to move. To minimize the energy of the system they start to self-assemble into the lowest energy structure. The structure formed can differ by changing the concentration, evaporation speed or the environment of the particles [17] [18].

Self-assemblies can also form at the interface of two different liquids, for example liquid-liquid [3] [14] [15]. Recent simulations of particles at a liquid-liquid interface have been performed [14]. Cubic particles with a homogenous interaction with the liquid were self-assembled on the interface and showed that two stable self-assemblies could be obtained with one of the particles facets {111} upward. The two self-assemblies that were calculated were a hexagonal and honeycomb lattice. The formation of these lattices are ascribed to capillary forces induced by the particles at the interface [14]. These two lattice have also been experimentally confirmed in literature, however here the driving forces are ascribed to ligand adsorption and van der Waals interactions [3] [15].

Oriented attachment

Oriented attachment can take place in the formation of anisotropic nanostructures [10] [19]. Oriented attachment is the connection of two nanocrystals by a specific crystal facet. This process takes place during crystal growth [10] and in bio-mineralization [20]. Some of these structures are nanowires and nanosheets [21]. Oriented attachment requires nanocrystals of uniform shapes and sizes, monodisperse particles with the same three dimensional shape. These monodisperse particles have well defined crystal facets. The well-defined crystal facets are required for oriented attachment [3].

Most nanocrystal are covered in surfactant molecules and they have a different binding energy for different facets. This allows for tuning of the reactivity of certain facets. Recently control over the oriented attachment of lead chalcogenides nanocrystals has led to superstructures with peculiar specific structure [2] [3].

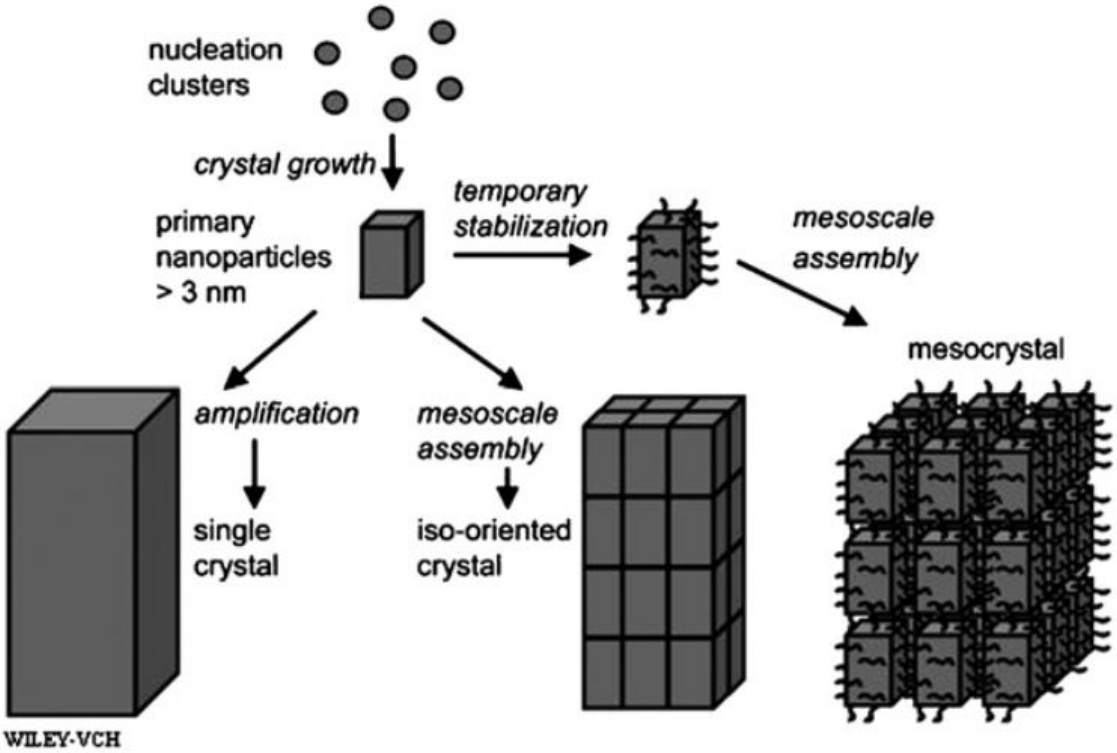

Figure 5. Schematic representation of the classical crystallization process the left and middle pathway. These kind of crystals grow via direct attachment of the primary nanoparticles. The pathway on the right is the oriented attachment pathway. The mesocrystal formed can fuse toward the middle structure (iso-oriented crystal) by loss of the ligands [22].

Most oriented attachment mechanism happen in a certain order of things. First a solution of monodisperse nanocrystals is needed. Next a self-assembly is needed of the nanoparticles for post synthesis oriented attachment. This self-assembly can be a large array of particles or a growing structure were new unattached particles draw closer and later attach. The schematic in Figure 5 gives the mechanism proposed for two or three dimensional attachment. The pathway on the right of the figure is the oriented attachment pathway. First a self- assembly is formed of multiple nanocrystals. The nanocrystals don't attach immediately, because the ligand prevents them from getting to close to each other (self-assembly). By removal of the ligands the nanoparticles can approach each other and form the final crystal, sometimes by first forming a neck between the particles [2].

Research on semiconductor structures has shown that the amount of ligands can influence the formed final structure by changing repulsion strength of different facets. J. Choi et al. [18] show that by creating structure under different atmospheric conditions they received two different final structures, FCC or BCC. They ascribe this difference to the loss of less tightly bound ligands at the surface of the nanocrystals.

To go from the self-assembly to an oriented attached structure the nanoparticles need to fuse together. Ligands can be removed using different method. In the some experiments where they form oriented attached structures on a liquid substrate it is proposed part of the ligands detach into the substrate and therefore making the surface free to attach [2] [3] [15]. Other experiments have shown that by adding a solvent [23] or treating a film of self-assembled particles [24] using a ligand detaching agent can also lead to attachment of particles. The attachment can also happen during the high temperature synthesis, by oriented agglomeration at a specific facet [19].

During the process of oriented attachment multiple forces are involved. The nanocrystals are covered with ligands and the steric hindrance of the ligands can be described as a repulsive force for the oriented attachment as has been stated above in the nanocrystal synthesis section. There the ligands have the function of stabilizing the nanoparticles against dissolving and colloidal aggregation [8] [10]. The ligands therefore also reduce the chance of oriented attachment and has also been studied in literature [3].

One of the attractive forces is surface area reduction, this is also the driving force for the aggregation of uncoated particles. This has been described in the synthesis of nanocrystal section above. There is has been stated that larger are more stable then small particles [10].

In oriented attachment the particles fuse in a controlled method using a specific crystallographic facet. The facets of a nanocrystal have different energies, for example in PbSe the {100} facets have the lowest energy followed by the {110} and {111} facets [25]. This would mean that attachment of the {111} facets would be the most energetically favourable. However high energy facets are covered with the most ligands and therefore the higher repulsive force makes it harder for attachment to take place. Attachment is therefore more likely at the facets with the lowest ligand coverage as the repulsive force will be the lowest. Simulations on the process of oriented attachment has shown that dipole-dipole interactions are not one of the main driving force in oriented attachment [25] [26].

For the formation of square attached superstructure of PbSe a mechanism has been proposed [15]. In this mechanism first a hexagonal self-assembly of the particles is formed. This self-assembly over times changes into a square self-assembly, due to ligands dissolving in the liquid substrate and the facet-facet interaction increasing. After this square assembly has formed the particles start attaching to form a square superstructure.

Experimental methods

Chemicals

Table 1. Table shows all the chemicals that were used, the abbreviation used for the chemical, the manufacturer and the purity of the chemical.

Chemicals	Abbreviation	Manufacturer	Purity
Lead acetate trihydrate	/	Sigma Aldrich	99,9999%
Octadecene	ODE	Sigma Aldrich	90%
Oleic acid	OA	Sigma Aldrich	90%
Tellurium powder	/	Sigma Aldrich	99,997%
Trioctylphosphine	TOP	Sigma Aldrich	90%
Ethylene glycol anhydrous	EG	Sigma Aldrich	99,8%
Ethanol anhydrous	EtOH	Alfa Aesar	96%
Hexane anhydrous	Hex	Sigma Aldrich	95%
Tetrachloroethylene anhydrous	TCE	Sigma Aldrich	≥99%

Lead telluride nanocrystal synthesis

The synthesis of the lead telluride (PbTe) quantum dots was based on the procedure of J. E. Murphy et al. [12]and J. J. Urban et al. [5]. All synthesis steps were performed in a nitrogen purged glovebox or on the shlenkline to prevent contact with oxygen.

First the two precursors were synthesized. The lead precursor was synthesized using 1,138 grams of lead acetate trihydrate, 3,30 mL of oleic acid and 8 mL of 1-octadecene. These chemicals were put in an Erlenmeyer and degassed und vacuum for 3 hours at ±130^{0}C. The solution will start to bubble because acetic acid is formed and due to the high temperature and vacuum this evaporates. After the synthesis is complete the solution was colourless to slightly yellowish. After a few days the solution turned into a white solid. The telluride precursor was made by dissolving 0,194g of telluride powder in 3 mL TOP. This was heated to ±70^{0}C and stirred until all the powder had dissolved. The solutions turned a yellow greenish colour when the telluride was dissolved.

For the synthesis of the nanoparticles the lead precursor was transferred into a three neck flask and heated till 170^{0}C. When the lead precursor had reached 170^{0}C the telluride precursor was quickly

injected. The solution turned black due to the formation of particles. The particles were allowed to grow for 3 to 5 minutes at 140^{0}C.

In some of the synthesis the temperature after the injection had risen till 155 ^{0}C and afterward cooled down to 140 ^{0}C and this temperature was maintained till 3-5 minutes had passed. After the growth time had passed the reaction was quenched by adding 3 mL of hexane. Next the solution was allowed to cool down to room temperature when they weren't treated further.

The particles were precipitated using 5 mL of ethanol and were centrifuged for 5 min at 2500 RPM. The supernatant was remover and the particles were redispersed in 5 mL of hexane. The washing step was repeated one more time.

Passivation of PbTe quantum dots

A couple of batches of nanoparticles were treated further based on the method of J. Y. Woo et al. [6]**.** In this paper the stability of lead selenide (PbSe) was increased considerably in comparison with untreated PbSe nanoparticles by use of a simple ammonium halogen treatment. The PbTe nanocrystals were treated directly after the growth of the particles and quenching of the reaction. The temperature was maintained at 60 ^{0}C for 15 min after 1 mL of a halogen solution (0,161 M Cl, Br or I) was added. This solution was made by dissolving an ammonium halogen powder in 10 mL of methanol. After this time the nanocrystals were washed using the same method as described above.

The success of the passivation treatment was measured by exposing treated and untreated particles to air. A zero point measurement was done by measuring the absorption spectrum of unexposed particles, both treated and untreated. Next the particles were exposed to air and measured after a couple of hours or days. The experiment was continued until the particles started precipitating or no exciton peak was visible anymore.

Oriented attachment

The oriented attachment experiments were based on the experiments performed by M. P. Boneschanscher et al. [2] and W. H. Evers et al. [3]**.** In these papers PbSe nanocrystal were used to form superlattices with a square or hexagonal structure. These experiments were performed on a liquid substrate of ethylene glycol (EG).

The experiments performed in this thesis were performed in a nitrogen purged glovebox. Petri dishes (27mm Ø) were filled with 6,6 mL of ethylene glycol. A mixture of 10 µL of oleic acid dissolved/mixed in 3 mL ethylene glycol (OA/EG) was also made. The amount of OA/EG used in the experiments ranged from 5 µL till 30 µL. in the experiments the OA/EG mixture was allowed to homogenise/ spread over the ethylene glycol substrate for 10 min. Afterwards the particle solution was added to the petri dish.

The temperature during the reaction was controlled using a cooling and heating plate. The atmosphere could also be controlled by placing a lid on the cooling and heating plate. This option to control the control the atmosphere was not available during this thesis, it could only isolate the petri dishes from the rest of the glovebox. The lid was used in experiments to create a saturated hexane atmosphere.

After one hour tem sample were made by scooping the superstructures at the surface onto a TEM grid. The surface of the ethylene glycol regularly showed flakes of some structure at the surface.

Absorption measurements

The absorption spectrum of the PbTe quantum dots was measured using a Perking Elmer Lambda 950 UV/Vis spectrophotometer. For the absorption measurements the particles were dispersed in TCE. In order to disperse the particles in TCE the particles were first dried under vacuum to evaporate the hexane and then redispersed in a volume of TCE.

By measuring the NIR absorption spectrum of PbTe particles the size of the particles can be determined. Due to quantum confinement effects also the oxidation of the particles can be studied, oxidation causes the PbTe crystal core to become smaller and therefore the absorption spectra blue shifts.

Transmission electron microscopy

Transmission electron microscopy (TEM) has been used to determine the size and ordering of the particles and their superstructures. The TEM images were made using a FEI Tecnai-10 and FEI Tecnai-12 Transmission Electron Microscope. With TEM also electron diffractions are measured in order to confirm the crystal structure of the superstructure. From this data the long range order of the structures can be determined.

Results & discussion

Quantum dot synthesis

PbTe quantum dots were successfully synthesized using the hot injection method. Directly after the hot-injection the solution turned black. After washing the particles they were analysed using absorption spectrum and a TEM. TEM samples were made by putting a droplet (10µ) of a diluted particle solution on a TEM grid and allowing this to dry.

In Figure 6 a typical absorption spectrum is shown. In the spectrum two peaks are visible. The lowest energy peak (highest wavelength) is the first exciton peak. The position of this peak can give the size of the nanoparticles. The shape of this peak and the rest of the spectra can give an indication of the size distribution and oxidation. Sharp and well defined peaks mean that the size distribution is narrow and there is little to no oxidation of the particles. The second peak (lower wavelength than the first exciton peak) is the second exciton peak. When this peak is visible it means the particles have a low polydispersity and that the particles are not oxidized or very little.

The appearance of multiple peaks in the absorption spectrum means the nanocrystals are in the strong confinement regime. Here discrete energy levels start to form at the edge of the band gap. This discrete energy levels lead to the appearance of the first exciton peak, band gap. The second exciton peak is the absorption of the second discrete level, which has a higher energy gap then the bandgap. Therefore the second exciton peak is measured at higher energy (lower wavelength).

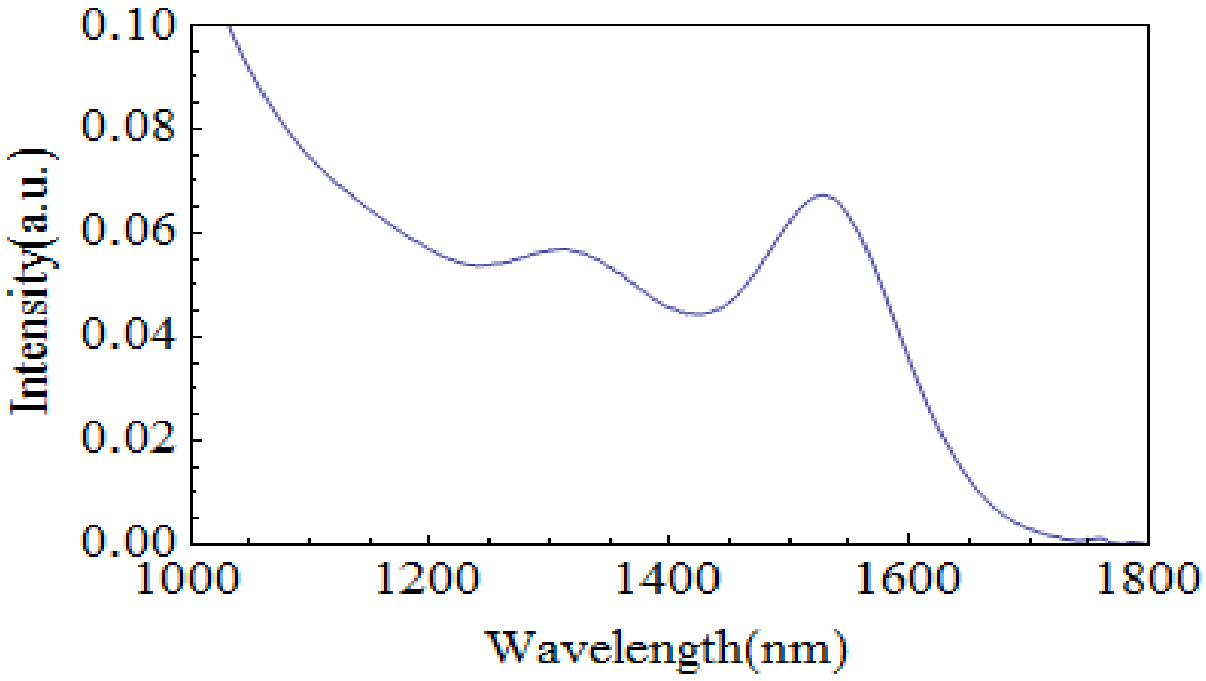

Figure 6. Absorption spectrum of MCT04W, it shows 2 peaks, the first exciton peak at around 1530 nm and the second exciton peak around 1110 nm. The appearance of two peaks means that the size distribution is small and the sharpness of the first exciton peak means the same.

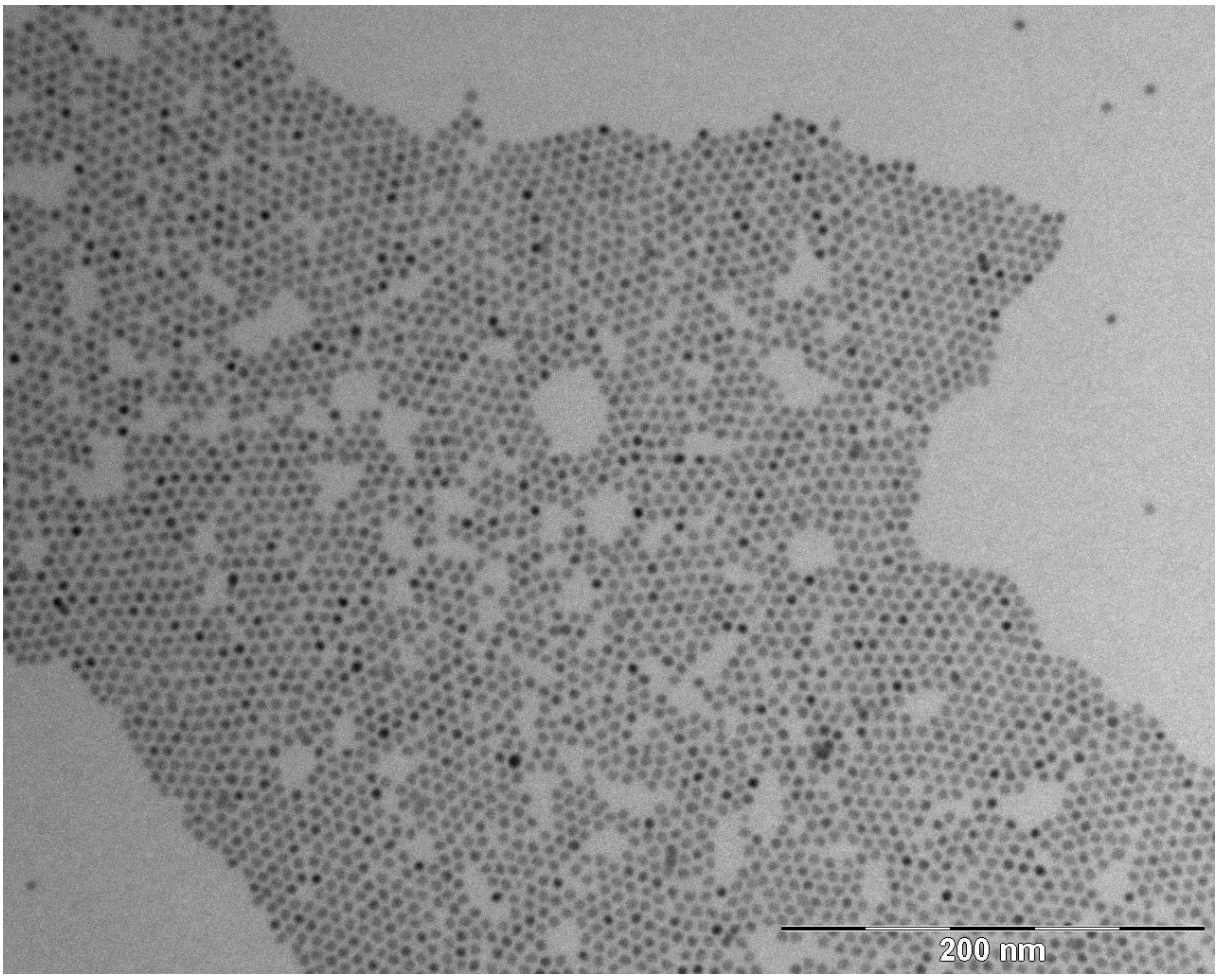

Figure 7. TEM picture of MCT04 with a mean size of 4,96 nm, and the picture shows hexagonal self-assembly of a large amount of particles meaning that the particles are monodisperse.

In Figure 7 a TEM image of a typical quantum dot sample (MCT04) is shown. The sizes of the most used particles are in the order of 5 nm. When the dots self-assemble in a hexagonal pattern over a longer length scale it says something about the monodispersity of the particles. The shape of the particles looks the same and after analysis the size and size dispersion can be determined. Some more measurements of the particles synthesized are shown in Appendix 1, quantum dot properties.

Passivation

A couple of batches of PbTe nanocrystals were passivated using halogen ammonium salts. The halogens chlorine, bromine and iodine were used. The particles were slightly bigger than their unpassivated particles, those who weren't treated further after the formation. This was checked by keeping part of the particles from the synthesis untreated for comparison. Next the first exciton peak position was followed through time.

The oxidation of PbTe quantum dots starts at the surface and then moves inward. Therefore the quantum confinement effect becomes greater, the crystal core becomes smaller. This shifts the first exciton peak to smaller wavelengths, higher energy. This has been explained in the quantum confinement part of the theory section.

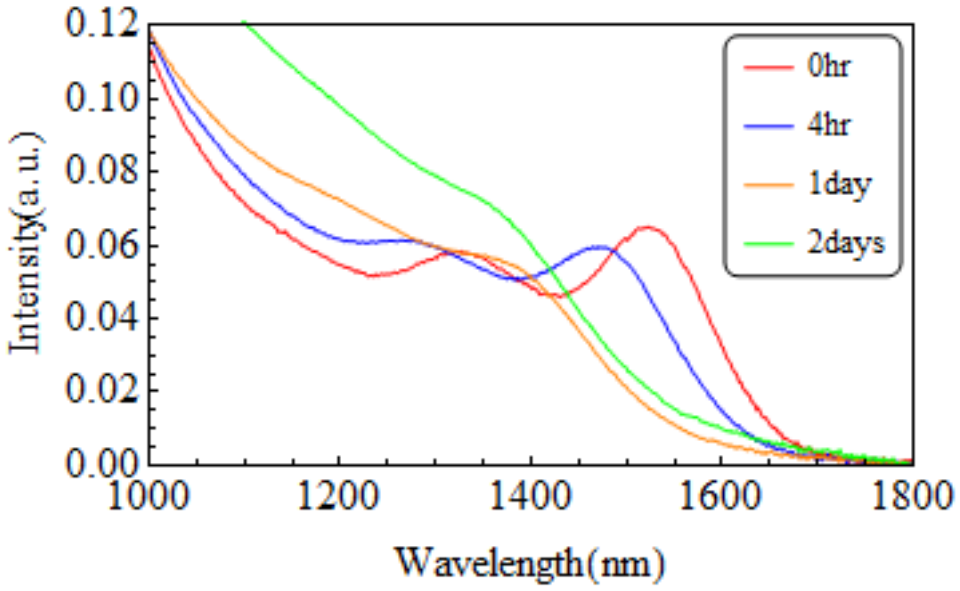

Figure 8. evolution of the absorption spectrum MCT04 (PbTe nanocrystal treated with chloride) after exposure to ambient conditions, the first exciton peak shifts to lower wavelengths and the second exciton peak is not visible anymore after 1 day.

The results of this process is shown in Figure 8 for chlorine passivate particles. It is visible that the entire spectrum shifts to lover wavelengths over time. The peak width at half maximum (FWHM) of the peak also increases over time, this can be seen by the broadening of the peaks. The broadening of the peaks is most likely due to different oxidation speed of the particles and therefore the cores sizes starts to differ. After a couple of days the particles started to lose their colloidal stability, the started to precipitate from the solution. The experiment were stopped at that moment, to protect the cuvets from being coated with precipitated particles.

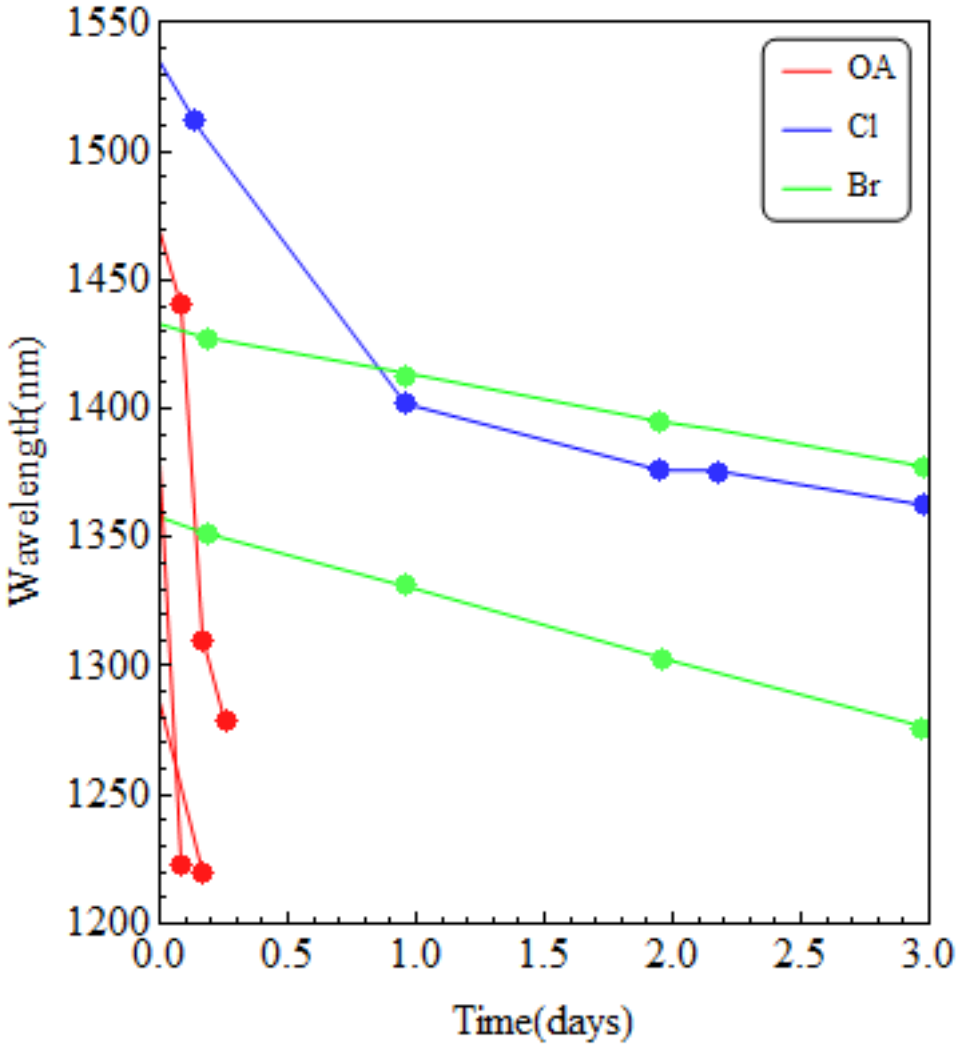

Figure 9. In this image an overview of the position of the first exciton peak is shown followed through time in air. This peak shifts to lower wavelength due to oxidation. The colour indicate what is used to passivate the particles. The points represent the measurement point and the lines have been drawn through those point to visualize the different oxidation speed. From the lines it's visible that bromide passivated particles oxidize the slowest, followed by chloride and that particles only with OA oxidize the fastest.

In Figure 9 an overview of all the passivated particles is shown. The slope of the graph gives the first exciton peak shift over time. The particles which were not passivated, named OA in Figure 9, show a very high shift in a short time. Meaning that these particle oxidize quickly and can't be used anymore in future experiment after a short exposure to air.

Particles passivated using chlorine show a decreased oxidation rate, smaller shift in the same time as OA in figure 9. It's also visible that the shift seems to slow down and stops after a couple of days. This is probably due to the formation of a thick oxidized layer at the surface which makes it more difficult for oxygen to reach the unaffected crystal in the core.

Bromine passivated particles show a linear decay of the first exciton peak position over time. This indicates that the particles still oxidize but the speed at which this happens is lower than chloride and untreated particles. This means that the particles still oxidize but a short exposure to air is less damaging.

The passivation was also performed using iodine. This wasn't successful, the particles lost their colloidal stability and the spectrum was distorted and broad, more information about the treatment with iodine and the spectra of the bromide treated samples are shown in Appendix 2, Passivation.

Oriented attachment

A large variety of oriented attachment experiment were done. Most of these experiment were performed using PbTe particles passivated with chloride and a size of about 5 nm (MCT04). These particles were also washed one more time using ethanol for a large amount of the experiments (MCT04W). The TEM picture and absorption spectra from these particles are shown above in the quantum dot synthesis section. These particles were chosen based on results obtained from a few trial experiment at the start of this thesis. These particles showed the best structures, less oxidized and more ordered and were therefore used further.

During the thesis multiple superstructures were synthesized: linear, square and honeycomb. These results were obtained using two oriented attachment methods: with extra OA on the ethylene glycol or without extra OA. The experiments with the added OA shows the best results and the biggest patches of structure. Therefore only at the start of the project experiments without OA were performed and led to more open structures.

The added OA should in principle make the spreading of the nanoparticles more homogeneous. Ethylene glycol isn't a good solvent for the particles and the added OA to the ethylene glycol gives the ethylene glycol surface a slight more favourable interaction with the particles. In the theory is has been shown that these structure form from a self-assembly. When this self-assembly is disordered the formed structure will also be more disordered. Also as described in literature [15], the rate at which oleic acid desorbs from the surface of the particles is lowered, which slows down the attachment speed and thus the time to form a self-assembly is increased. The higher homogeneity of the particles at the surface should give a more homogeneous final structure and thus on a larger scale.

The experiments were done in the glovebox with an O_2 concentration of about 4ppm, these values fluctuated. The O_2 concentration was measured using an oxygen analyser or DEZ (diethylzinc), DEZ start to smoke at around 4-5 ppm oxygen.

The concentrations listed will be based on the dilution of the PbTe solution, the real concentration of PbTe was not known because no data on the extinction coefficient of PbTe could be found in literature. In Appendix 1, quantum dot properties the concentration of the solution is calculated based on the extinction coefficient of PbSe, this concentration will probably be in the same order of magnitude based on the large similarities in the bulk crystal absorption spectra [27] [28].

Experiments have also been performed where the temperature was raised or lowered slightly (10^{o}C). changing the temperature didn't lead to bigger patches of superstructure and raising the temperature only lead to stronger attached particles, less necking, and more disorder in the structure. Some final experiments were performed under a saturated hexane atmosphere. These experiments showed large self-assemblies of particles which contained hexagonal, pseudo-hexagonal and square lattices.

Square structure in the size order of 100-200nm could be synthesized with a reproducibility of about 60%, estimated from all the images using the same conditions. Honeycomb and linear structures were also obtained, but these results were not reproducible.

Electron diffraction have been taken from some of the formed superstructures. A six fold symmetry is visible for the honeycomb structure and a fourfold symmetry for the square (percolative) lattices. Due to the small size of the square patches and the honeycomb patches, the diffractogram only confirms we have a square or honeycomb lattice. For the square structures the symmetry is only visible by integrating the powder ring and plotting the intensities. For the honeycomb patches a pinhole was used to zoom onto the structure and only focus on the honeycomb part to obtain the electron diffractogram. Due to this the electron diffraction only consist of a couple of points. These electron diffractions are shown in Appendix 3, electron diffraction.

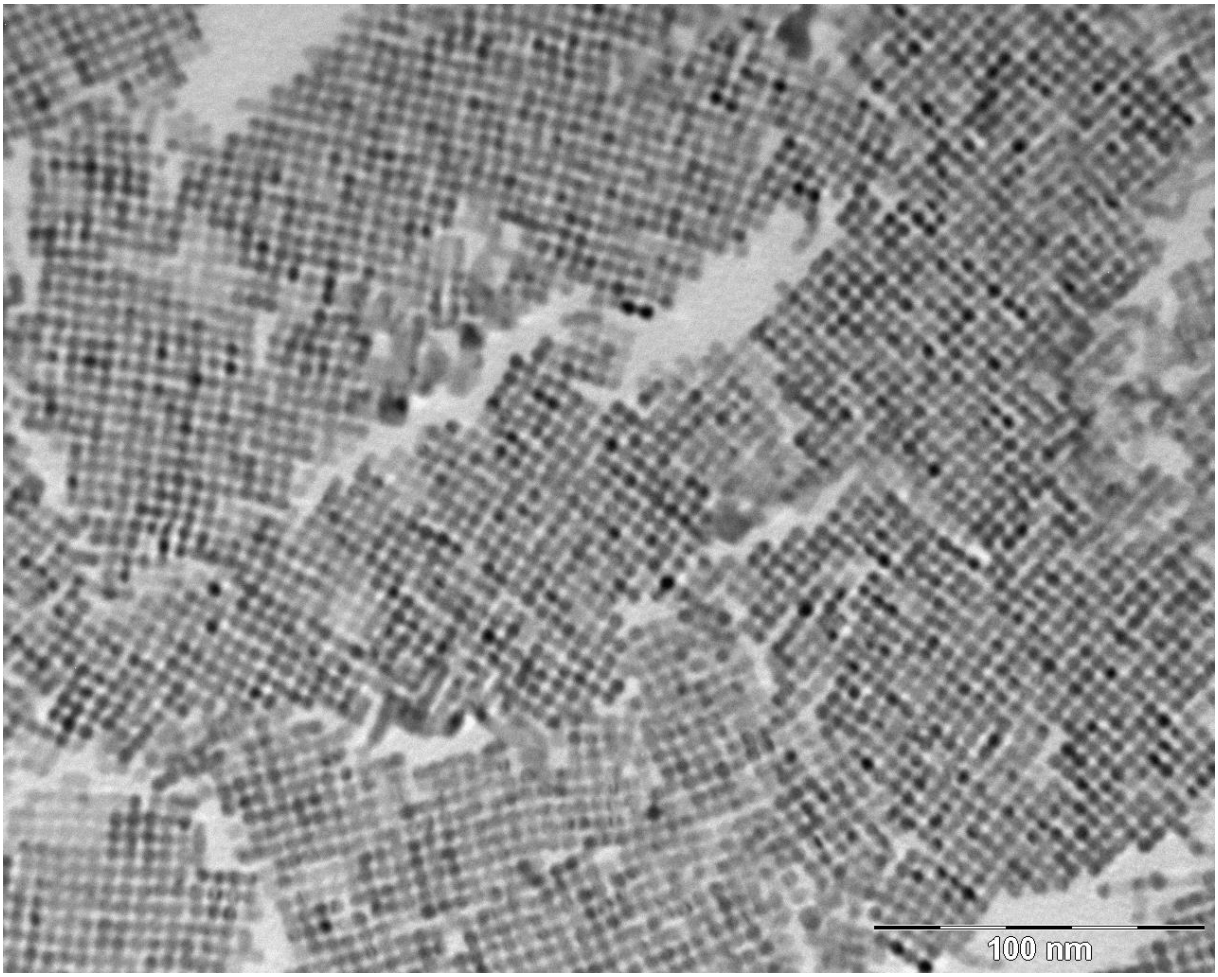

Figure 10. TEM image of square superlattices synthesized using MCT04W diluted 200 times. Multiple patches of square superlattices are shown, with a size in the order of 100-200nm. The particles aren't completely attached there is a neck in between the particles.

For all the experiments 6,6 mL of ethylene glycol was put in a petri dish. To synthesize the large square structure 15 µL of OA/EG (10 µL OA in 3 mL EG) mixture was added to the ethylene glycol and allowed to homogenize for 10 min. The PbTe particles were diluted 200 times and an amount of 350

µL was put on the EG. After one hour a TEM sample was scooped from the surface of the ethylene glycol, the surface showed some flakes of brownish structures.

Using the above described method and a sufficiently clean glovebox, oxygen concentration below 4 PPM square structures similar to the structure shown in Figure 10 could be synthesized reproducible. The reproducibility of these structure was approximately 60%. This percentage was estimated by looking at the structures obtained using these conditions.

As can be seen in the figure the structure isn't one large structure but multiple different patches of similar size. The formation might be due to the nature of PbTe. PbTe is the most reactive of the lead chalcogenides and looks to attach very rapidly. This rapid start of attachment might disrupt the formed self-assembly and therefore crystalize into multiple patches. Necking is also visible in the figure which has also been seen in literature. [3]

Before these large square structures were obtained different structures were synthesized. In Figure 11 a TEM image of one of these experiments is shown. It shows a square like structure, to be more precise a percolative square lattice. These structures were obtained by a more diluted particle solution, in the order of 500-600x diluted. Also there was no extra oleic acid added to the ethylene glycol.

The formation of these structures is likely due to the lower concentration, lower concentration means less particle which can attach and form the superstructure. The particles are also stronger attached to each other in comparison, this might also be due to the lower concentration or due to the atmosphere in the glovebox. The amount of oxygen fluctuated regularly during these experiments and this can also explain the very open unordered structures in between the parts of ordered structures. The coverage of these structures on the TEM was low, most likely due to the low amount of nanoparticles used. In some of the more disordered parts of these structures small honeycomb patches had formed. This unordered parts with honeycomb were more dense, more particles during the formation of the structure.

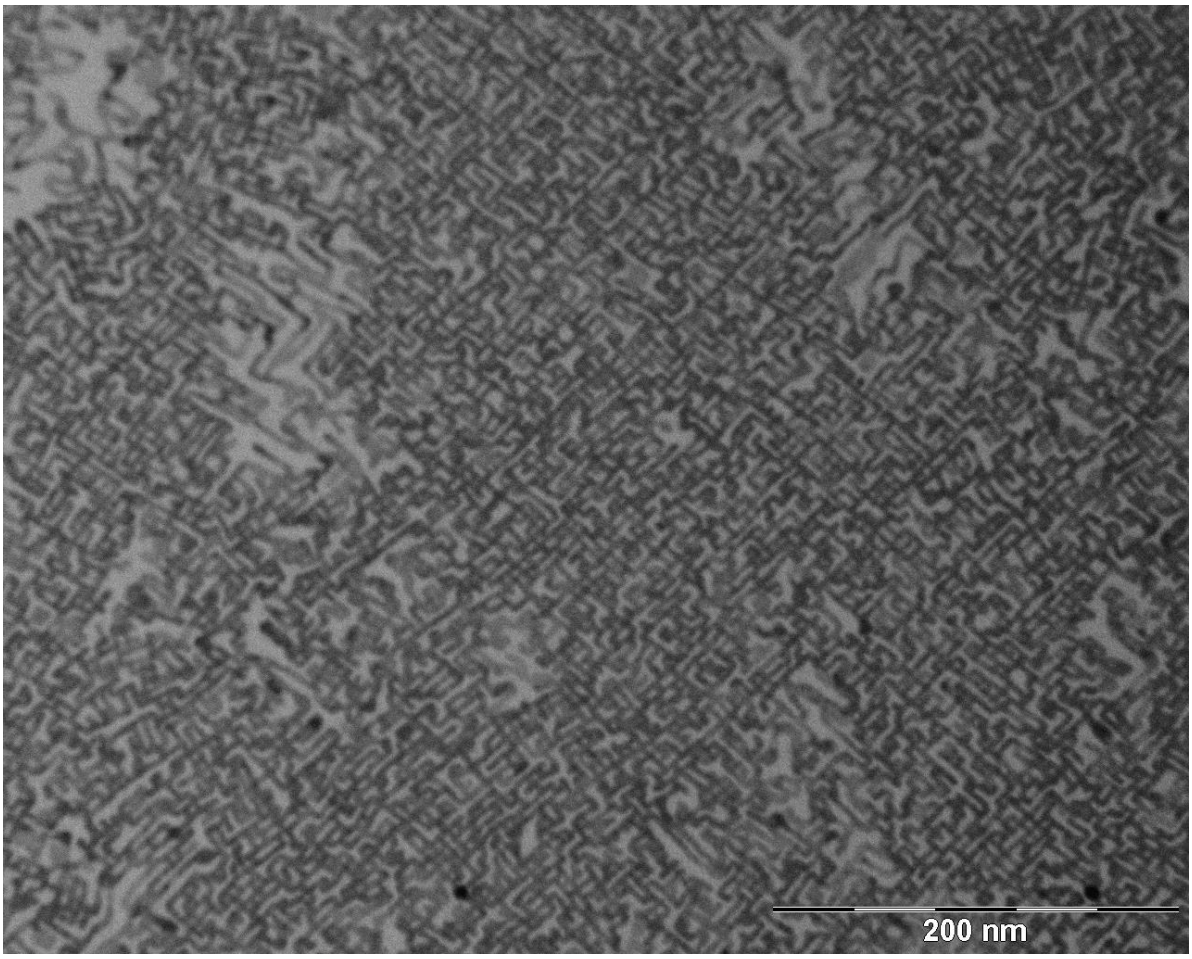

Figure 11. TEM image of square percolative lattices, made using MCT04 with a dilution of 600 times. The particles are stronger attached to each other in comparison with Figure 10, no necking is visible anymore. There are also part visible with linear like structures which look quite unordered, this is likely due to oxidation.

When OA was added to the EG substrate larger square superstructure as described above and shown in Figure 10 were obtained. However in some cases also large honeycomb structures were obtained. .When the experiments contained a high amount of honeycombs structures, these honeycomb structures had similar patch sizes (100-200nm) to that of the square superstructures.

These results had no reproducibility and were therefore not obtained very often. One of these results is shown in Figure 12. It is visible that is has a large patch of honeycomb structures. These structures were not dominant on the entire TEM sample, other parts contained small patches of square and honeycomb structures.

The honeycomb samples mostly contained a lot of unordered structures or unattached particles. This might be due to the fact that the honeycomb structure require a denser self-assembly and that the dots have to be oriented differently on the substrate. According to literature the honeycomb structures have their {111} facet pointed away from the ethylene glycol [2], instead of the {100} facet for the square structure [3] [15].

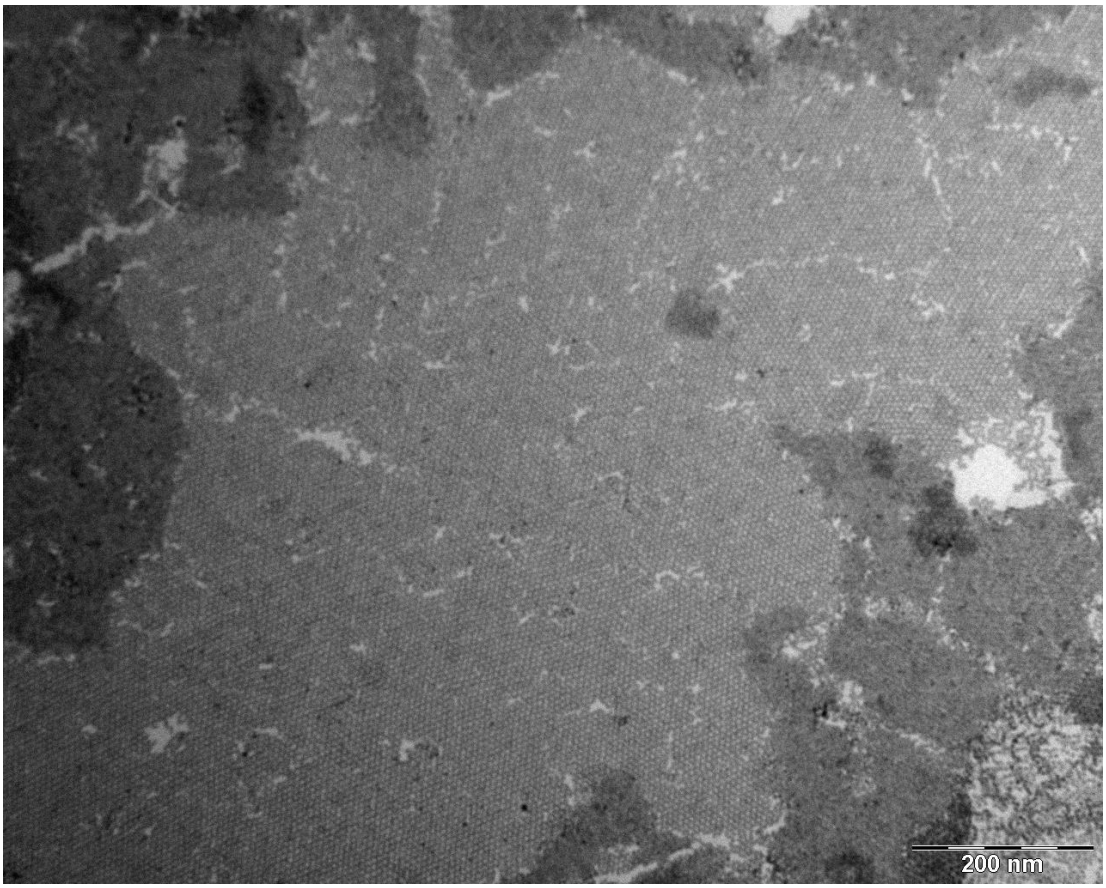

Figure 12. TEM picture of honeycomb structures, synthesized using MCT04W diluted 200 times. The honeycomb patches have similar sizes to the square superstructures shown in Figure 10. Al these honeycomb patches are surrounded by double layers and unordered structures.

At a certain moment a setup was build which allowed for a great control of the temperature. The setup contained a heating and cooling plate and a glass cover which could be closed airtight. The temperature could be maintained at a constant within $0{,}02^0$C of the set temperature. Using this setup experiments were performed at lowered temperature and higher temperature.

By changing the temperature the speed at which the solvent evaporates can be controlled and therefore the time for the particles to form a self-assembly or attach. The idea was that by lowering the temperature PbTe would attach less quickly and therefore be able to make bigger structure by allowing the particles to have more time to make a self-assembly and approach each other. By raising the temperature the self-assembly will have less time to go from a hexagonal lattice to a square lattice. This could allow easier formation of the honeycomb superstructure, which form from a hexagonal self-assembly lattice.

The experiments performed at lower temperature still showed attachment, but the obtained structures were not larger or more homogeneous. Both the honeycomb structures and square structures were obtained at both higher and lower temperature and no increased amount of honeycomb superstructures were formed at higher temperatures. Some TEM pictures of these experiments are shown in Figure 13 for lowered temperature and Figure 14 for higher temperature**.**

For the experiments at lower temperature less OA has to be added to the EG surface or else the particles had trouble attaching into larger structures, lots of unattached were seen in experiments with similar amounts as the large square structures at room temperature.

In Figure 13 an example of a TEM picture of structures obtained at lowered temperatures is shown. There are a lot of square patches visible in the picture, but there size is smaller than the structures obtained at room temperature, about 50nm compared to 100-200nm. Small linear structures are also visible in between the patches of square structure. When linear structures were obtained these always were short, less than 50 nm long. This is different in comparison with PbSe were also very long attached linear structures could be obtained [3].

At higher temperature the problem is that the oriented attachment goes to fast leading to unordered structures as seen in figure 14. This is most likely due to the fact that PbTe attaches even faster at higher temperatures and therefore the orientation is sometimes not correct. However the parts that were attached at higher temperature were more strongly attached, less necking was visible.

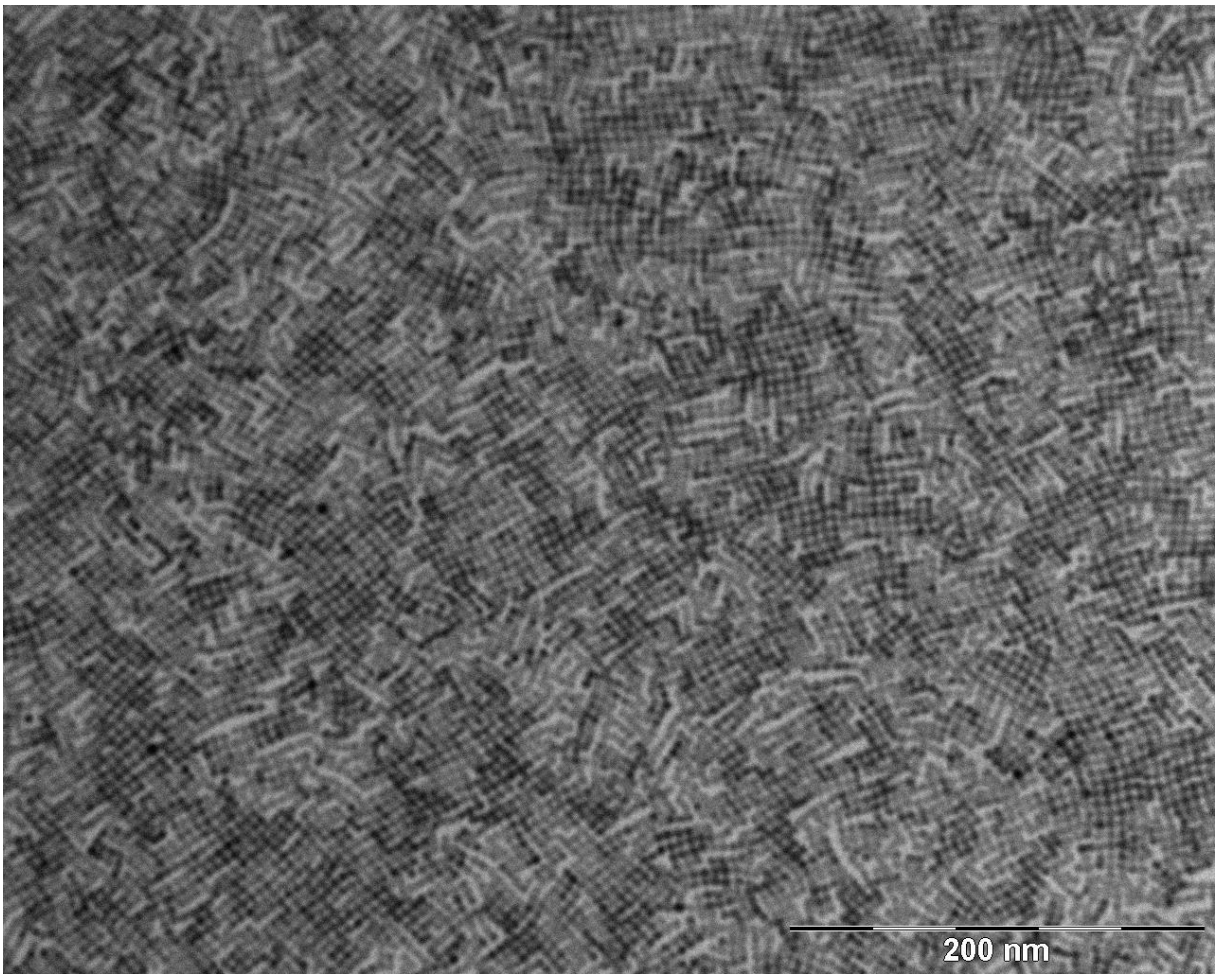

Figure 13. Square structured flakes synthesized at 10^0C using MCT04W diluted 200 times. A lot of small square patches are visible and small necks are visible between the particles. In other parts there were also unattached particles. Small linear structures are also visible in between the square superstructure patches.

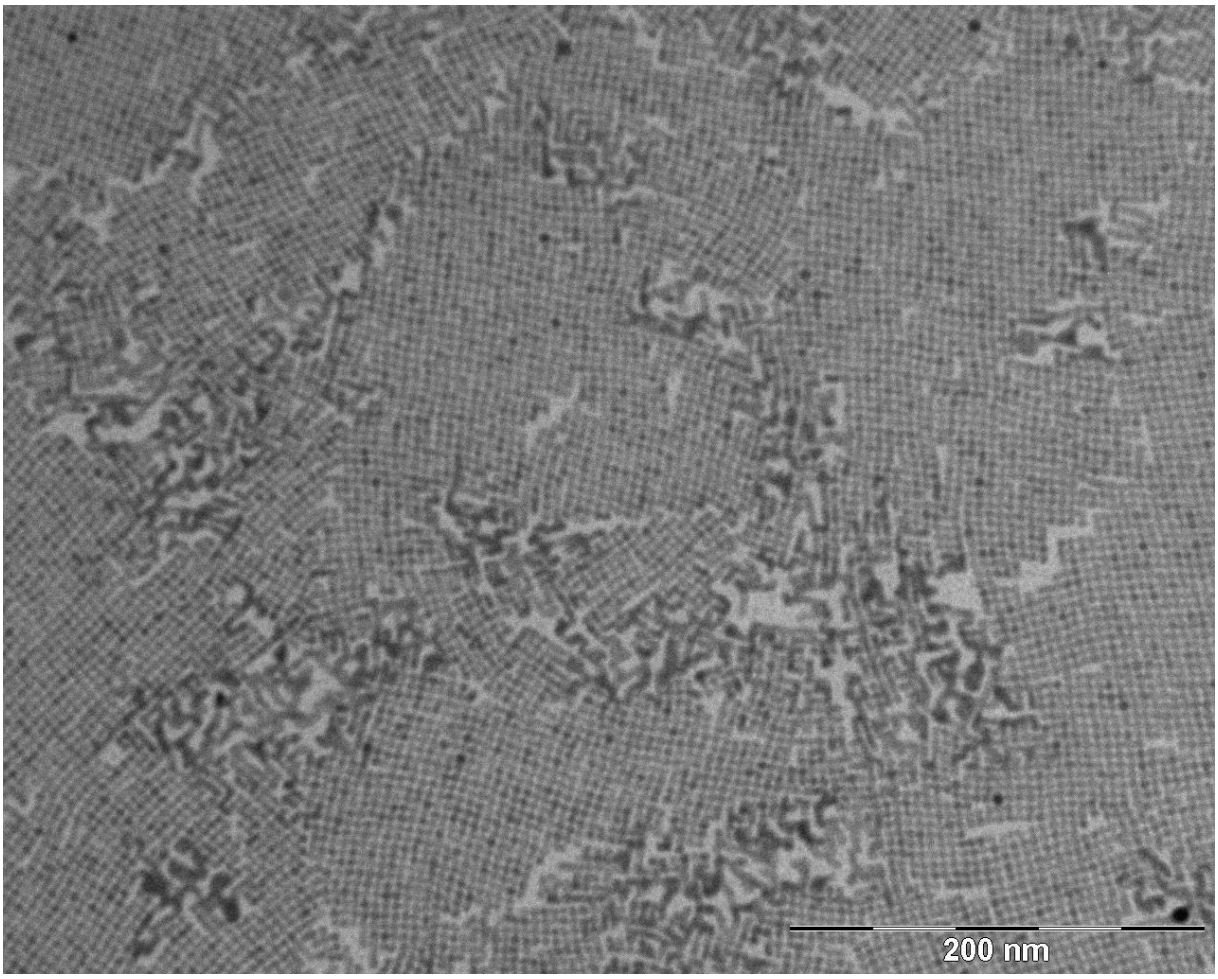

Figure 14. TEM picture of structures formed at 25^{0}C using MCT04W diluted 210 times. Mostly square structures were obtained, no increase in the amount of honeycomb superstructures. The square structures obtained are of similar size or slightly smaller than the structures obtained at room temperature. At higher temperature more unordered structures are visible.

Almost all the previous structures were synthesized on the bottom of the glovebox. When trying to imitate the experiment on the bottom using the setup. By using the same temperature as the bottom, measured by a thermometer, and using the same synthesis amounts. These experiments showed that the structures synthesized on the bottom are slightly better and show less unordered structures. When using the setup also two petri dished were used at the bottom of the glovebox to mimic the experiments in the setup. This might be due to the fact that the experiments performed using the setup are quite high of the bottom of the glovebox, which might lead to slight difference in the atmosphere (solvent or oxygen concentration for example). Vibrations are clearly visible in the ethylene glycol on the setup when working inside the glovebox or walking around in the same room.

Some final experiments were performed using the setup cover and using petri dishes filled with hexane. These petri dishes filled with hexane were put inside the cover together with petri dishes with ethylene glycol and oleic acid. Next the cover was closed using caps and parafilm. After ten minutes a QD solution was added to the ethylene glycol. This way small attached structures were obtained and also self-assemblies of the dots. These structures are shown in Figure 15 and Figure 16. The oriented attached structures look a bit like ‘Tetris’ pieces, they consist of a couple of dots till

structure of about 100 nm. The self-assembled particles show patches of particles oriented in a similar way. Some of these patches have a hexagonal order and some a more square/pseudo hexagonal like assembly.

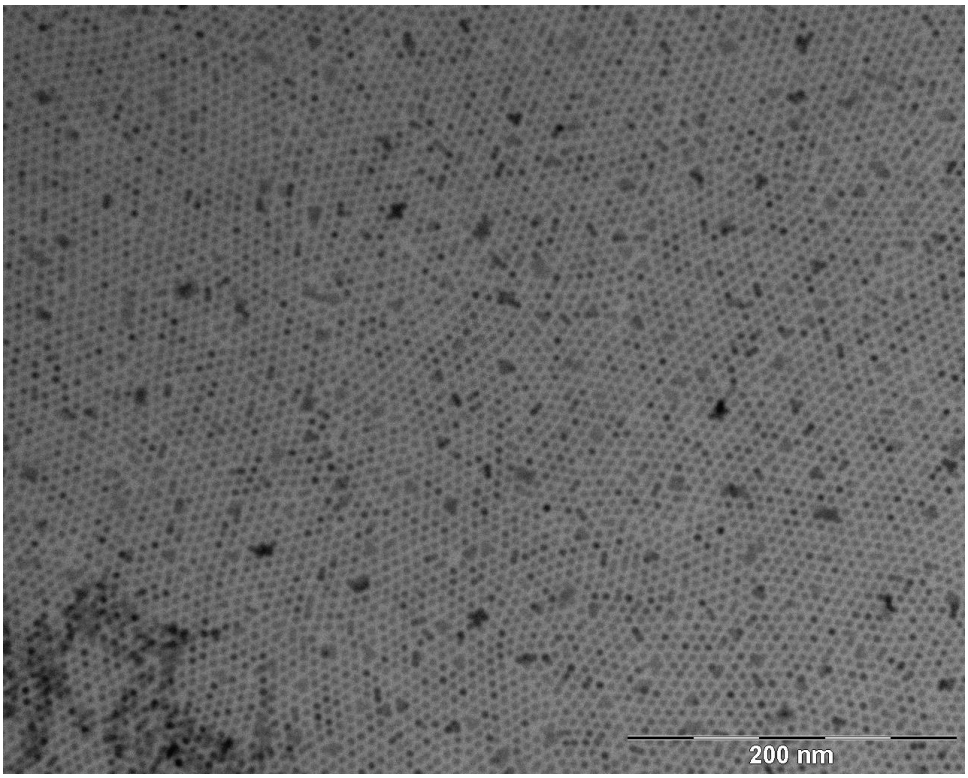

Figure 15. Self-assembly obtained by using a saturated hexane atmosphere while synthesizing superlattices. During the synthesis MCT04W was used diluted 220 times. In the picture different patches of self-assemblies are visible: hexagonal, pseudo-hexagonal and square. This was in the same sample that also contained small attached structures.

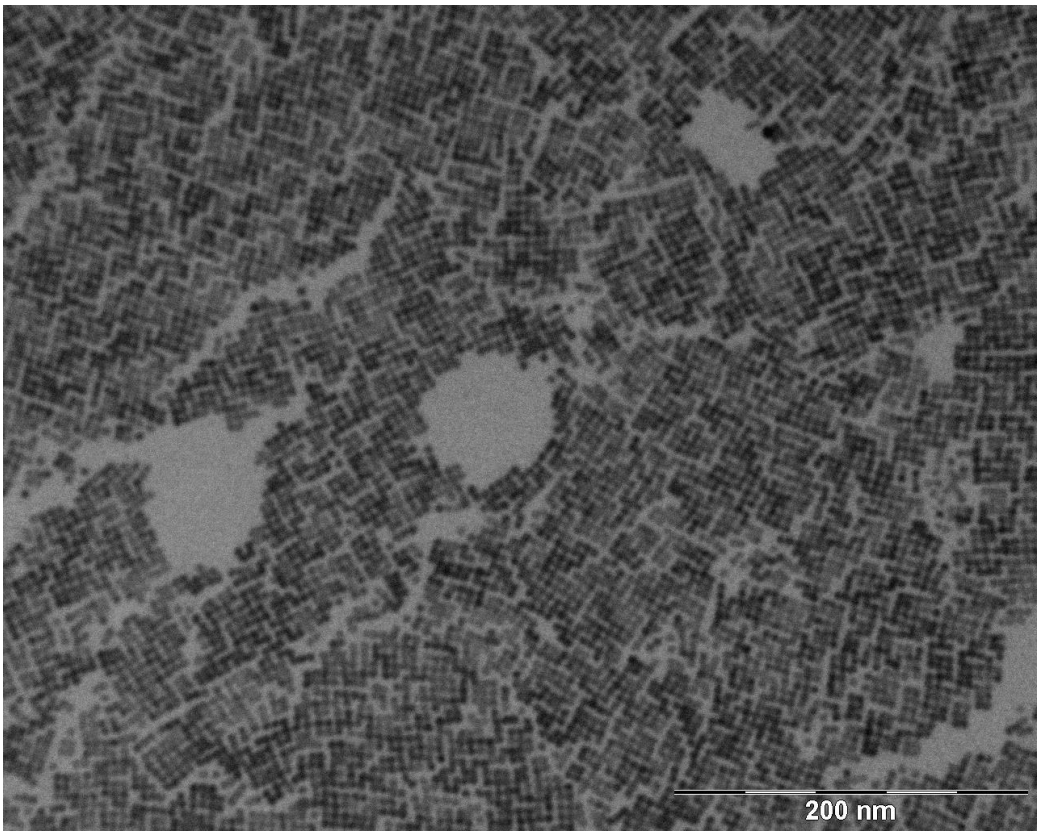

Figure 16. Structures made using a closed setup under a more solvent concentrated atmosphere. 220x diluted MCT04W was used with 2 Petri dishes of hexane next to the samples in the setup. A lot of small patches of square superstructure are visible. Some of these very small patches are arranged together in a similar direction.

Conclusion

We managed to synthesize PbTe nanocrystals of different sizes. These particles show multiple absorption peaks and form hexagonal self-assembly in TEM and are therefore monodisperse. PbTe is very easily oxidized by oxygen therefore the nanoparticles were passivated. The PbTe nanoparticles were passivated using ammonium halogen salts and the effect of this treatment was investigated using absorption spectroscopy. The absorption peaks were followed through time while the particles were exposed to ambient conditions. The particles were passivated using chloride and bromide.

The experiments shows that bromide treatment is the most promising in regards to passivation against oxygen. It still shows oxidation but at a significant lower rate than chloride and bare particles. Treatment using iodide seemed to decrease the colloidal stability of the particles, they started agglomerating within a few days after synthesis. The absorption spectra also changed due to this agglomeration and therefore the data was not usable.

Next also oriented attachment experiments were performed. These experiments show that PbTe quantum dots can attach in three different kinds of structures, ranging from linear structures to square and honeycomb structures.

The structure that could be synthesized the most reproducible was the square superstructure with a patch size of about 100-200nm. For this synthesis method OA was added to the EG substrate and an

oxygen concentration of below 4PPM was required. These structures remained patchy, this might be due to the fast attachment of the particles or a too high polydispersity of the particles which distorts the self-assembly. These square superstructures of 100-200nm can be synthesized with a reproducibility of about 60%, based on the experiments performed and analyzing the TEM data.

More open square structures were also synthesized using a lower concentration of particles for the oriented attachment experiments. These structure show stronger particle-particle attachment and only very limited necking. The low amount of necking might also be due to the condition inside of the glovebox, the concentration of oxygen fluctuated a lot. Oxygen distort the forming structures by oxidizing the particles and therefore altering the surface of the particles. PbTe nanocrystal themselves are the least stabile in the lead chalcogenides family and therefore they react the easiest.

This can also be seen in the oriented attachment experiments, almost in all the experiments there is attachment. At the start of my attachment experiments there were also some signs of honeycomb patches, these were mostly only visible in dense distorted patches on the TEM grid. Also in experiments where OA was added to the EG honeycomb structure could be obtained in the order of 100-200nm. These honeycomb structures couldn't be made reproducible.

Changing the temperature didn't lead to more honeycomb structures or larger square structure. Lowering the temperature lead to smaller patches of square structures compared to room temperature. This might be due to lower amount of attachment of the particles. Raising the temperature lead to stronger attached particles, but also more unordered and random attached structures.

Finally, oriented attachment experiments were performed where the atmosphere was saturated using Petri dishes filled with hexane. Using this and normal attachment conditions self-assemblies as well as small Tetris like attachments were obtained. Already in these self-assemblies grain boundaries can be seen and also different kind of self-assemblies, square/pseudo hexagonal and hexagonal.

Outlook

We succeeded in synthesizing square superstructures of 100-200 nm with a reasonable (60%) reproducibility. To increase the size of the superstructures or the reproducibility of the method changing the atmosphere to a cleaner atmosphere might help. PbTe is the most sensible lead chalcogenide to oxygen, therefore less oxygen is less oxidation and more ordered structures.

No electronic measurement have been performed on these structures and this might be interesting. This could validate the simulation performed in literature [4] [29]. Only near the end of the project the temperature control setup was ready and after my practical work was done it became possible to work under a cleaner nitrogen atmosphere (bip quality nitrogen). Doing more experiment under a constant and controlled temperature and cleaner atmosphere might lead a better reproducible result. PbTe even after the passivation treatment that was performed PbTe still oxidizes faster than PbSe and oxygen distorts the structures formed significantly.

During the project only hexane was used as a solvent but hexane evaporates fairly quickly and it might be interesting to do attachment experiment with slower evaporating solvent. This could slow down the evaporation speed and lead to larger patch sizes. Slower evaporation of the solvent gives more time to form a self-assembly at the ethylene glycol substrate. However toluene, as used for PbSe oriented attachment experiments, damages the PbTe quantum dots and causes them to dissolve or fall apart.

Lowering the temperature didn't lead to larger patch size or a purer structure. A lower temperature gives a slower evaporation speed and thus more time to form a self-assembly. The experiments showed that the attachment of the particles became too weak or slow to make large structures.

To compare the stability more precisely multiple batches of the same size of nanocrystals would have been required. The synthesis can be controlled quite well for sizes up to about 5 nm using the method I have described above. To synthesize larger particles the growth time should be increased or the excess of oleic acid reduced.

For the superstructure synthesized using PbSe it has been proven that the PbSe superlattices can be converted to a CdSe superlattice by cation exchange. It might be interesting to do this also for the PbTe structure and see if the superstructures survives the treatment. This would then also give a route to form CdTe and maybe different Te based superstructures. CdTe has a different electronic structure compared to PbTe and might there be interesting for different applications.

Bibliography

[1] A. K. Geim and K. S. Novoselov, "The rise of graphene," *Nature materials,* vol. 6, pp. 183-191, 2007.

[2] M. P. Boneschanscher, W. H. Evers, J. J. Geuchies, T. Altantzis, B. Goris, F. T. Rabouw, S. A. P. van Rossum, H. S. J. van der Zant, L. D. A. Siebbeles, G. Van Tendeloo, I. Swart, J. Hilhorst, A. V. Petukhov, S. Bals and D. Vanmaekelbergh, "Long-range orientation and atomic attachment of nanocrystals in 2D honeycomb superlattices," *Science,* vol. 344, no. 6190, pp. 1377-1380, 2014.

[3] W. H. Evers, B. Goris, S. Bals, M. Casavola, J. de Graaf, R. van Roij, M. Dijkstra and D. Vanmaekelbergh, "Low-Dimensional Semiconductor Superlattices Formed by Geometric Control over Nanocrystal Attachment," *Nano letters,* vol. 13, pp. 2317-2323, 2013.

[4] E. Kalesaki, C. Delerue, C. Morais Smith, W. Beugeling, G. Allan and D. Vanmaekelbergh, "Dirac cones, topological edge states and nontrivial flat bands in two-dimensional semiconductors with a honeycomb nanogeometry," *Physical review x,* vol. 4, p. 011010, 2014.

[5] J. J. Urban, D. V. Talapin, E. V. Shevchenko and C. B. Murray, "Self-Assembly of PbTe Quantum Dots into Nanocrystal Superlattices and Glassy Films," *Journal of the American Chemical Society,* vol. 128, pp. 3248-3255, 2006.

[6] J. Y. Woo, J.-H. Ko, J. H. Song, K. Kim, H. Choi, Y.-H. Kim, D. C. Lee and S. Jeong, "Ultrastable PbSe Nanocrystal Quantum Dots via in situ Formation of Atomically Thin Halide Adlayers on PbSe(100)," *Journal of the American Chemical Society,* vol. 136, pp. 8883-8886, 2014.

[7] J. Zhang, J. Gao, E. M. Miller, J. M. Luther and M. C. Beard, "Diffusion-controlled synthesis of PbS and PbSe quantum dots with in situ halide passivation for quantum dot solar cells," *ACS Nano,* vol. 8, no. 1, pp. 614-622, 2014.

[8] C. d. M. Donegá, "Synthesis and properties of colloidal heteronanocrystals," *Chemical society reviews,* vol. 40, pp. 1512-1546, 2011.

[9] A. P. Alivisato, "Perspectives on the physical chemistry of semiconductor nanocrystals," *Journal of Physical Chemistry,* vol. 100, no. 31, pp. 13226-13239, 1996.

[10] C. de Mello Donegá, Nanoparticles workhorses of nanoscience, Springer, 2014.

[11] E. Groeneveld, Synthesis and optical spectroscopy of (hetero)-nanocrystals, Utrecht: Utrecht University, 2012.

[12] J. E. Murphy, M. C. Beard, A. G. Norman, P. S. Ahrenkiel, J. C. Johnson, P. Yu, O. I. Mićić, R. J. Ellingson and A. J. Nozik, "PbTe Colloidal Nanocrystals: Synthesis, Characterization, and Multiple Exciton Generation," *Journal of the American Chemical Society,* vol. 128, pp. 3241-3247, 2006.

[13] M. J. D. Lane and G. S. Grest, “Spontaneous asymmetry of coated spherical nanoparticles in solution and at liquid-vapor interfaces,” *Physical review letters,* vol. 104, pp. 235501-2235504, 2010.

[14] G. Soligno, M. Dijkstra and R. van Roij, “Self-assembly of cubes into 2D hexagonal and honeycomb lattices by hexapolar capillary interactions,” *Physical review letters,* vol. 116, pp. 258001-25006, 2016.

[15] J. J. Geuchies, C. van Overbeek, W. H. Evers, B. Goris, A. de Backer, A. P. Gantapara, F. T. Rabouw, J. Hilhorst, J. L. Peters, O. Konovalov, A. V. Petukhov, M. Dijkstra, L. D. Siebbeles, S. van Aert, S. Bals and D. Vanmaekelbergh, “In-situ study of the formation mechanism of two-dimensional superlattices from PbSe nanocrystals,” *Nature Materials,* 2016.

[16] L. Rossi, Colloidal Superballs, Utrecht, 2012.

[17] W. H. Evers, Entropy driven and reaction driven self-assembly of colloidal semiconductor nanocrystals, Utrecht, 2012.

[18] J. J. Choi, C. R. Bealing, K. Bian, K. J. Hughes, W. Zhang, D.-M. Smilgies, R. G. Hennig, J. R. Engstrom and T. Hanrath, “Controlling nanocrystal superlattice symmetry and shape anisotropic interactions through variable ligand surface coverage,” *Journal of the American Chemical Society,* vol. 133, pp. 3131-3138, 2011.

[19] K.-S. Cho, D. V. Talapin, W. Gaschler and C. B. Murray, “Desingning PbSe nanowires and nanorings through oriented attachment of nanoparticles,” *Journal of the American chemical society,* vol. 127, no. 19, pp. 7140-7147, 2005.

[20] J. F. Banfield, S. A. Welch, H. Zhang, T. Thomsen Ebert and L. R. Penn, “Aggregation-based crystal growth and microstructure development in natural iron oxyhydroxide biomineralization products,” *Science,* vol. 289, pp. 751-754, 200.

[21] C. Schliehe, B. H. Juarez, M. Pelletier, S. Jander, D. Greshnykh, M. Nagel, A. Meyer, S. Foerster, A. Kornowski, C. Klinke and H. Weller, “Ultrathin PbS sheets by two-dimensional oriented attachment,” *Science,* vol. 329, pp. 550-553, 2010.

[22] Q. Zhang, S. Liu and S. Yu, “Recent advances in oriented attachment growth and synthesis of functional materials: concept, evidence, mechanism and future,” *Journal of Materials Chemistry,* vol. 19, no. 2, pp. 191-207, 2009.

[23] K. Witham, J. Yang, B. H. Savitzky, L. F. Kourkoutis, F. Wise and T. Hanrath, “Charge transport and localization in atomically coherent quantum dot solids,” *Nature materials,* 2016.

[24] W. J. Baumgardner, K. Witham and T. Hanrath, “Confined-but-connected quantum solids via controlled ligand displacement,” *NANO letter,* vol. 13, pp. 3225-3231, 2013.

[25] C. Fang, M. A. Huis, D. Vanmaekelbergh and H. W. Zandbergen, "Energetics of polar and nonpolar facets of PbSe nanocrystals from theory and experiments," *ACS NANO,* vol. 4, no. 1, pp. 211-218, 2010.

[26] H. Zhang and J. F. Banfield, "Interatomic coulombic interactions as the driving force for oriented attachment," *CrystEngComm,* vol. 16, pp. 1568-1578, 2014.

[27] E. A. Albanesi, E. L. Peltzer y Blanca and A. G. Petukhov, "Calculated optical spectra of IV-VI semiconductors PbS, PbSe and PbTe," *Computational materials science,* vol. 32, pp. 85-95, 2005.

[28] C. E. Ekuma, D. J. Singh, J. Moreno and M. Jarrell, "Optical properties of PbTe and PbSe," *Physical Review B,* vol. 85, pp. 85205-85212, 2012.

[29] E. Kalesaki, W. H. Evers, G. Allan, D. Vanmaekelbergh and C. Delerue, "Electronic structure of atomically coherent square semiconductor superlattices with dimensionality below two," *Physical review B,* vol. 88, pp. 115431-115439, 2013.

[30] S. V. Gaponenko, Introduction to nanophotonics, Cambridge university press, 2010.

[31] D. Grodzinska, Colloidal PbSe/CdSe heteronanocrystals, Utrecht: Utrecht Univerity, 2012.

Appendix 1, quantum dot properties

The sizes of the particles were determined using TEM and the absorption spectra. From the data of the absorption spectra also the concentration can be determined if the extinction coefficient is known. For PbTe nanoparticles the extinction coefficient is not known, but to give an indication I have calculated the concentration using the extinction coefficient of PbSe. The coefficient is size dependent so the concentration calculated here might differ from the actual concentration [28] [27]. The results are shown in Table 2. The concentration data shows that all the particle have about the same concentration or are in the same order of magnitude.

Table 2. Table with the sizes of different batches of nanoparticles and concentrations calculated based on PbSe extinction coefficient.

Name	Size TEM (nm)	Size absorption (nm)	Concentration (mol/L)
MCT03	4,77	4,79	$1{,}051*10^{-5}/1{,}025*10^{-5}$
MCT04	4,96	4,98	$1{,}587*10^{-5}/1{,}562*10^{-5}$
MCT04W		4,97	$1{,}566*10^{-5}/1{,}501*10^{-5}$

MCT05	4,32	4,33	$1{,}327*10^{-5}/1.449*10^{-5}$
MCT06	4,05	4,04	$8{,}055*10^{-6}/8{,}973*10^{-6}$
MCT11	4,48	4,43	$1{,}176*10^{-5}$
MCT12	T12	4,62	$1{,}768*10^{-5}$
MCT13	T12	4,19	$1{,}076*10^{-5}$
MCT14	T12	4,45	$2{,}357*10^{-5}/2{,}487*10^{-5}$

An emission spectrum was also taken during the project to further check the properties of the particles synthesized. This spectrum was taken of MCT03 dissolved in TCE. The spectrum is shown in Figure 17**.** The emission peak position is slightly red shifted with respect to the absorption peak. That means that the nanoparticles are not oxidized and are crystalline. This measurement was performed using an Edinburgh Xe900 lamp and an Edinburgh Instruments FLS920 spectrofluorometer.

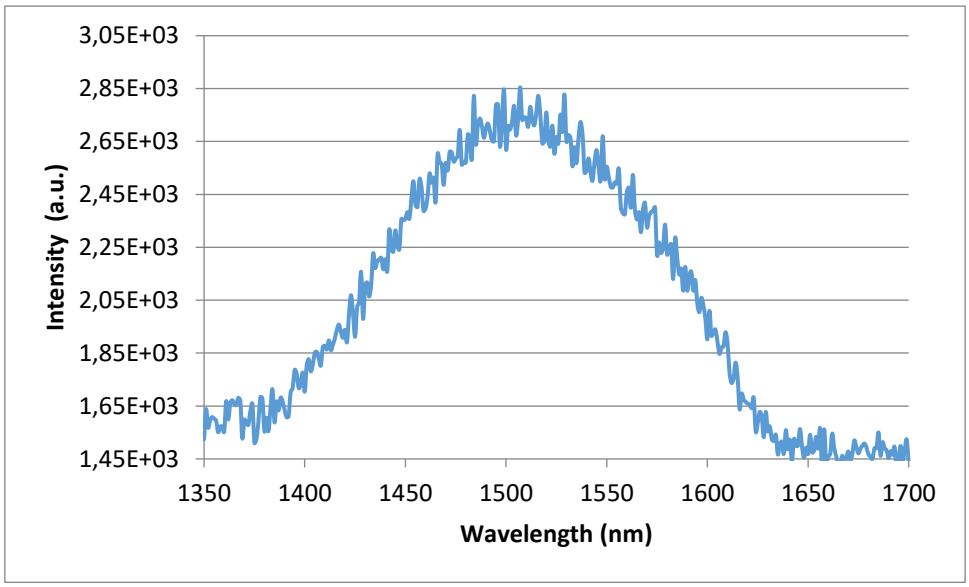

Figure 17. Emission spectrum of MCT03, measured in a closed cuvette particles dissolved in TCE.

X-ray diffraction measurements were also performed on some of the quantum dot samples. These samples were made by drying droplets of nanoparticles dissolved in hexane on a piece of glass. This piece of glass was cut from a microscope glass, the rest of the microscope glass was used as the sample holder for in diffractometer. The diffractometer used was a Philips PW 1729 X-ray generator and a Philips PW 3710 MPD control. The diffractogram is shown in Figure 18, it shows that all the peak are in good correspondence with the reference. There is a small shift visible, this is due to the reference being measured on bulk material and not quantum dots. In quantum dots the lattice contracts [10] and therefore the positions shift slightly.

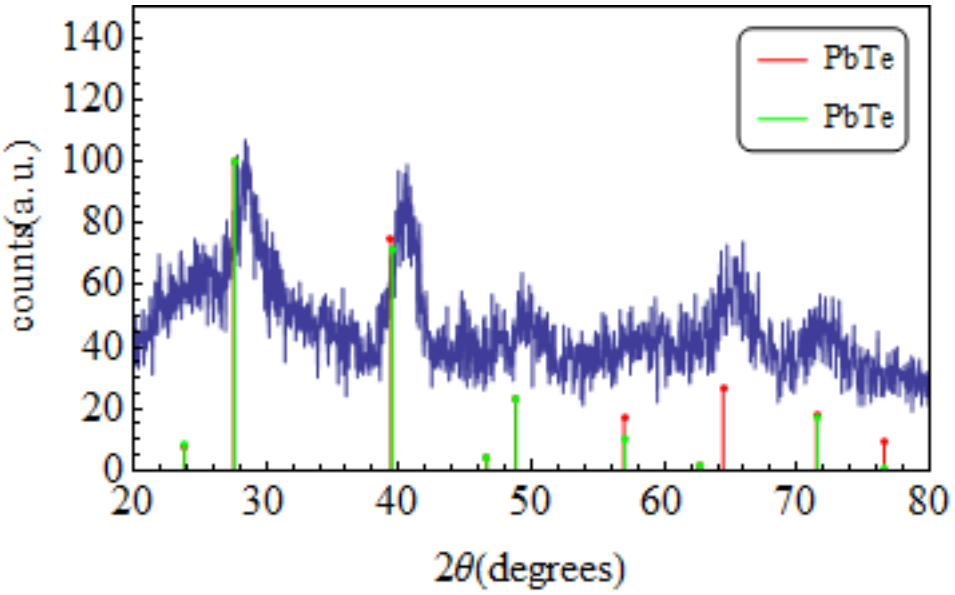

Figure 18. X-ray diffractogram of MCT03. The red and green lines correspond to two sets of reference data of PbTe. At the start of the diffractogram is a broad signal due to the piece of glass used as a sample holder.

Appendix 2, Passivation

As shown above in the results section the PbTe particles treated with bromide still oxidize but slower. The spectra are plotted together in Figure 19. The shift to lower wavelengths is visible and also a slight increase in intensity, possibly due to the increased background.

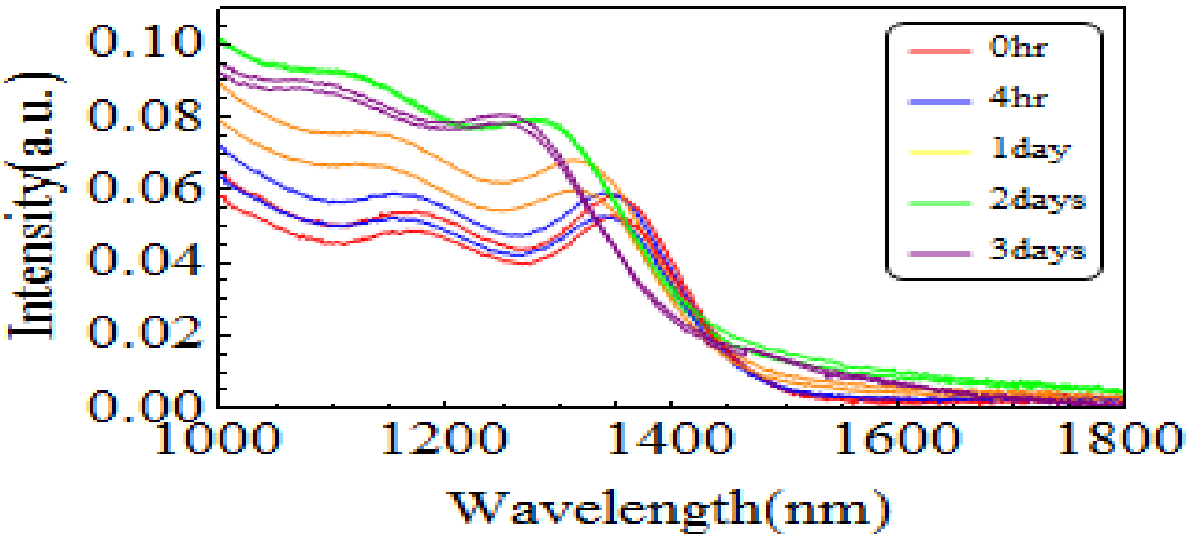

Figure 19. Evolution of the absorption spectra of MCT05, PbTe nanocrystal treated with bromide, exposed to air. It is visible that the peaks shift to lower wavelengths and that after 3 days both the first exciton and second exciton are still visible.

In Figure 20 TEM pictures and the day one absorption spectra are shown of MCT16, PbTe passivated using iodide. In the picture on the right you can clearly see separate particle. The particle appear to be less spherical than the other synthesized particles. A couple of days later, the particles had precipitated and as can be seen on the right TEM picture, the particles had aggregated. These two effect might explain what happened, they both seem to indicate that the oleic acid ligands have been removed to a very large extent and that the iodide isn't enough to stabilize the nanoparticles. It might also be possible that iodide isn't even bound to the surface of the quantum dots. Comparing the size of the quantum dots under TEM with the absorption spectrum measured on the day of the synthesis indicates that the particles have oxidized. The peaks are quite broad and also the size is calculated at 4,40 nm while TEM gives 5,15 nm. The absorption spectra of the clustered particles only give a peak around the peak around the same value, however higher energy peaks are not visible and the intensity is quite low. I predict the particles to be oxidized to such an extent that a thick enough shell of oxidized material has formed around a small PbTe core and that this still gives a signal in the spectrum. This is also visible in highly oxidized samples (PbTe with Cl after a few days), there is also still a feature visible in the spectra, but less pronounced and more shifted in the background absorption.

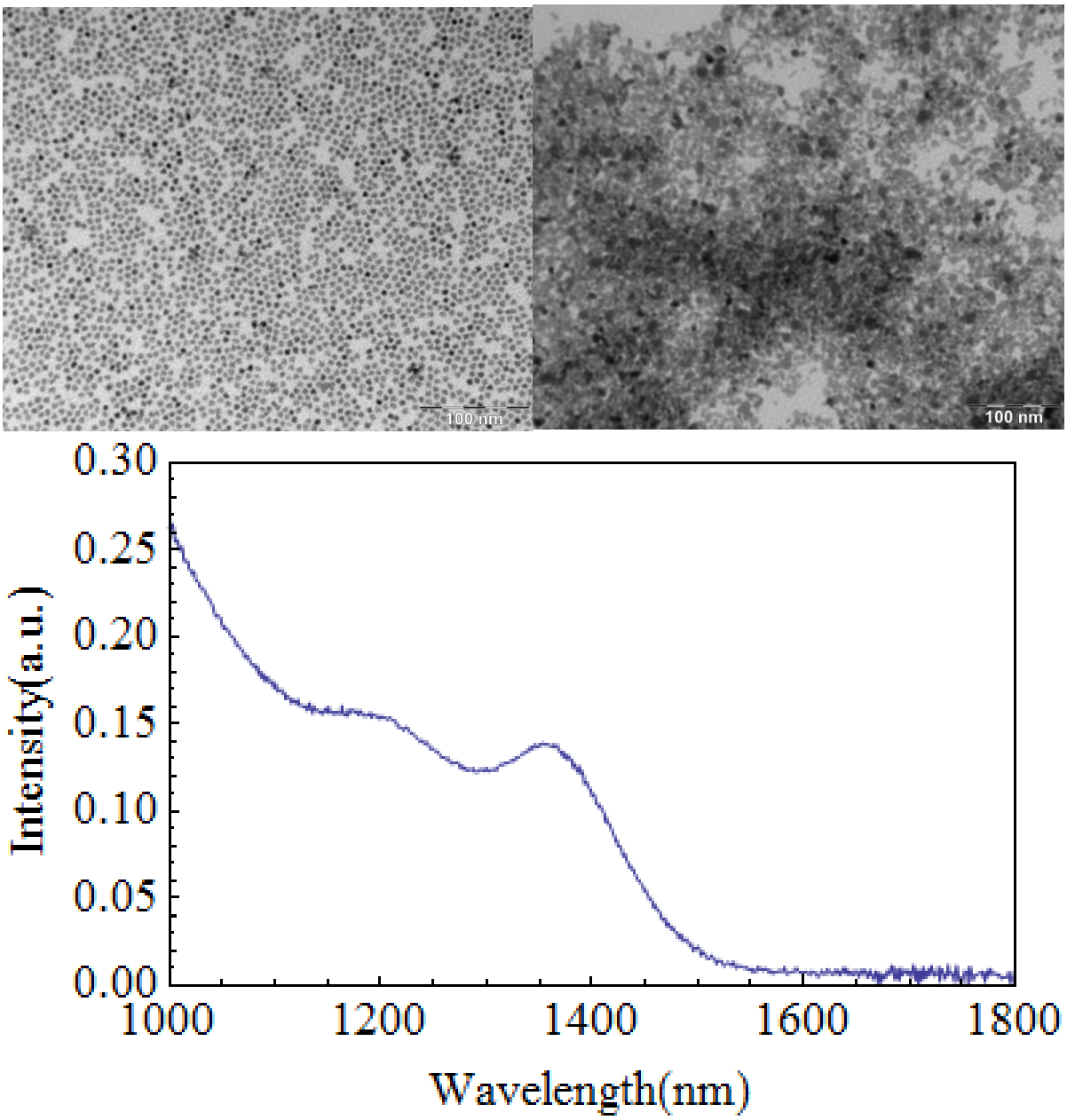

Figure 20. On the top left the TEM picture of MCT16 at day 1 after synthesis, on the right after the weekend. On the bottom the absorption spectrum is shown made on the day of the synthesis.

Appendix 3, electron diffraction

In this section some electron diffractions are shown and analysed. Most of the electron diffractions performed on the structures were not very clear. This was because of the limitation of the TEM. The FEI Tecnai-10 can only take electron diffractions of a large area. The structure synthesized are mostly on a smaller scale (100-200nm) than the electron diffraction area (a couple of µm). At the start of the project some electron diffractions were measured using the FEI Tecnai-12. This one can perform selective area diffraction and therefore focus on a small piece of the TEM grid. The structure at that time of the project were not very good and therefore only small structure were measured. One of these measurements is shown in Figure 21. This measurement has been taken on a small piece of honeycomb structure. This is also visible in the electron diffraction, because there are only a limited amount of particles there are also only few signals visible in the diffractogram.

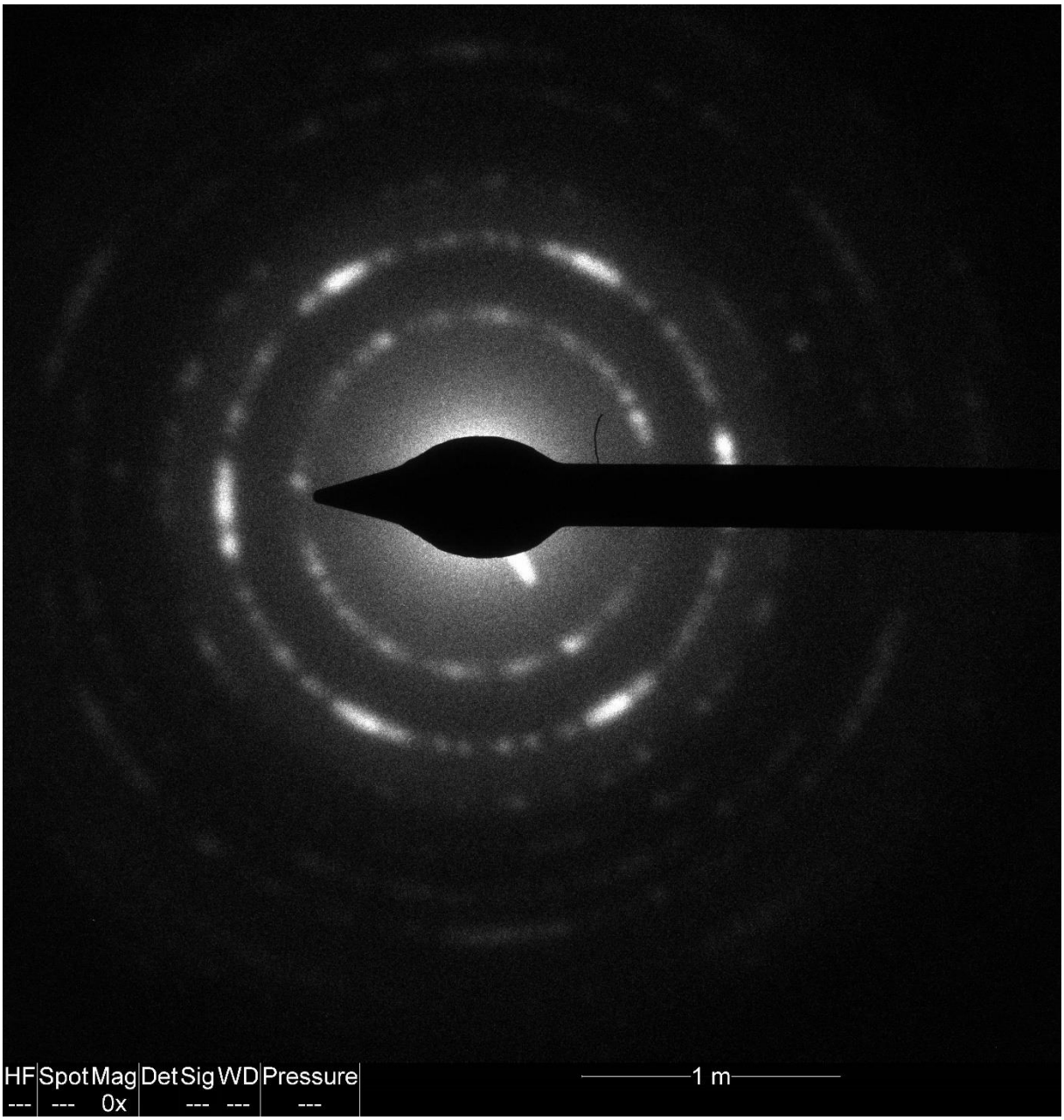

Figure 21. Electron diffractogram of a small piece of honeycomb structure

This electron diffraction is made of a small piece honeycomb structure. Also electron diffraction have been taken from pieces of square structure. This measurements were performed using the FEI Tecnai-10 and therefore the diffractogram doesn't show very clear peak. This TEM takes the electron diffraction of a very large area and therefore to see clear peaks the structure has to be periodic in a very large area.

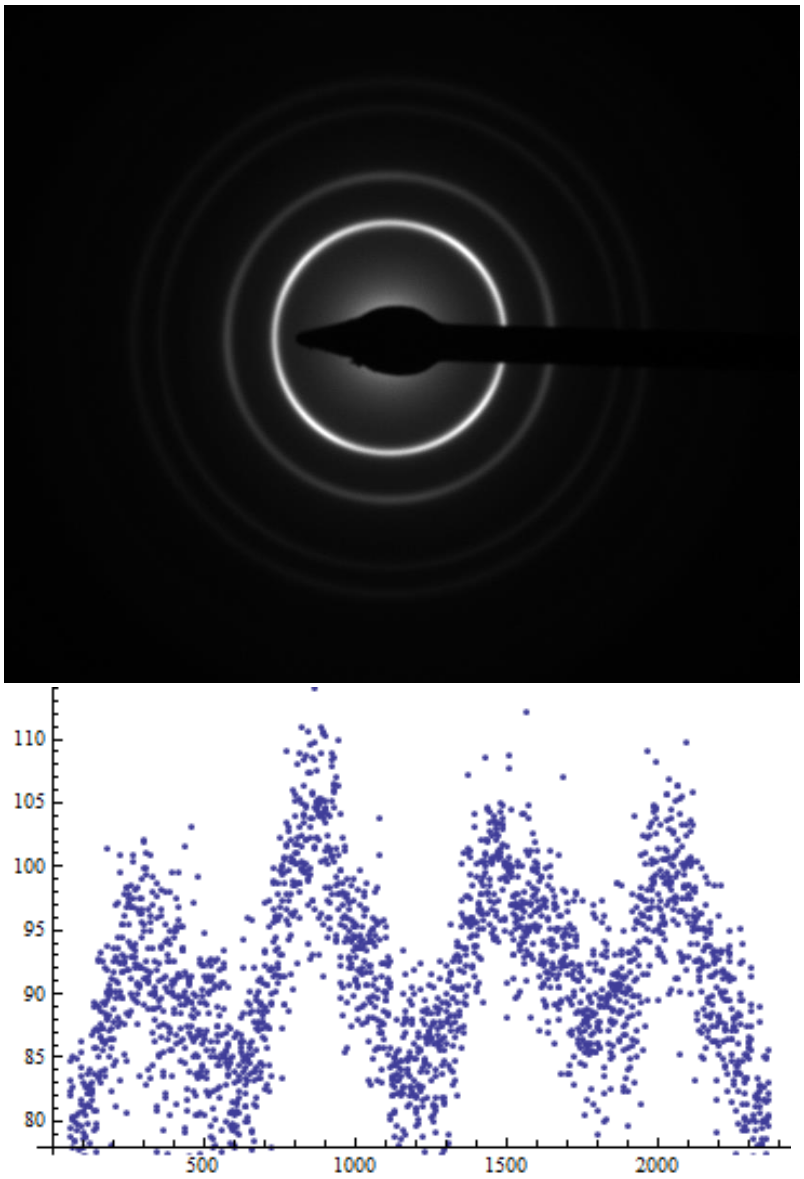

Figure 22. On the top the electron diffractogram of a sample of square structure, made with the FEI Tecnai-10. The position of the rings correspond with the diffraction signal of a square lattice. On the bottom the circular intensity plot is shown of the bright white circle, this plot shows 4 peak corresponding with a 4-fold symmetric structure.

By making a circular intensity plot the peaks can be made visible. This plot shows four peaks and corresponds well with the structure it is taken from. The position of the circles also correspond with the diffractions of a square lattice. The diffractogram and plot are shown in Figure 22 and the square structure is shown in Figure 11.

Appendix 4, oriented attachment database

Below a table is shown of all the oriented attachment experiments performed. The conditions used are noted in this table and also the results from the experiments. From looking through the result column it's visible that mostly square structure were synthesized sometimes also with other structures.

Table 3. Table with all the oriented attachment experiments. The dilution of the particle solution used and which particles were used is shown in column two. The amount of OA/EG added to the EG substrate is shown in column three. The temperature if measured is shown in column four and in the final column the general results of the experiment are reported.

Date	Concentration/dilution (MCT04/MCT04W was used unless stated otherwise)	µL OA/EG (10µL/3mL)	Amount of QD solution	Temperature	Result
8-4-2015	400x	0	350	??	Lines
8-4-2015	500x	0	350	??	Square / lines
8-4-2015	600x	0	350	??	Square / lines
8-4-2015	700x	0	350	??	Square / lines
29-4-2015	500x	0	350	??	not
29-4-2015	500x	5	350	??	much
29-4-2015	500x	15	350	??	interesting
8-5-2015	500x	0	350	??	lines
8-5-2015	500x	5	350	??	Small squares
8-5-2015	500x	15	350	??	Lines/ square
11-5-2015	500x MCT05	0	350	??	lines
20-5-2015	250x	0	350	??	Lines
20-5-2015	250x	30	350	??	Square / junk
20-5-2015	125x	30	350	??	Square / dots
From this moment MCT04W was used. this solution was made by washing 2 mL of MCT04 with 2 mL etOH and the particles were redispersed in 2 mL hexane					

29-5-2015	250x	15	350	??	Square / dot / line
29-5-2015	200x	15	350	??	Square / line / honey
29-5-2015	200x	20	350	??	Honey / dot
15-6-2015	200x	20	350	??	square
15-6-2015	150x	20	350	??	junk / square / honey
15-6-2015	200x	25	350	??	Square
29-6-2015	200x	15	350	??	Square
29-6-2015	200x	17	350	??	Honey ☺ / square
29-6-2015	200x	18	350	??	??
7-2-2015	200x	20	350	??	Square / dots
7-2-2015	200x	25	350	??	Honey or square
10-2-2015	200x	17	350	??	square
10-2-2015	200x	20	350	??	square
10-2-2015	200x	25	350	??	Square / dots
8-9-2015	200x	15	350	??	square
8-9-2015	200x	20	350	??	Square / dots
15-9-2015	250x	15	350	??	Square / lines oxidized
15-9-2015	250x	15(2uL OA / 14mL Hex)	350	??	Square / lines oxidized
15-9-2015	250x	0	350	??	Square / lines oxidized
02-10-2015	200x	15	350	18	Small squares
02-10-2015	200x	15	350	24-25	Square and molten structures

02-10-2015	200x	15	350	24-25	Square and unordered structures
7-10-2015	200x	15	350	10	Molten pieces, unordered structures and assemblies, some honeycomb
7-10-2015	250x (MCT14, likely partly oxidized using synthesis)	15	350	10	Mostly lines or molten structures and some square
7-10-2015	200x	15	350	23	Square structures
8-10-2015	200	10	350	10	Square, lines, some honeycomb
8-10-2015	250(MCT14, likely partly oxidized using synthesis)	10	350	10	xxx
8-10-2015	200	10	350	13 till 20	Honeycomb, unordered and small square
8-10-2015	250(MCT14, likely partly oxidized using synthesis)	10	350	13 till 20	xxx
14-10-2015	200	10	350	10	Small squares and unordered
14-10-2015	200	10	350	18 till 22	Some square and lines(small patches) and molten parts
14-10-2015	200	15	350	18 till 22	Squares, but also molten and disordered parts
16-10-2015	210	15	350	25	Small square, lines and molten/disordered parts

16-10-2015	210	15	350	20 till 21	Squares and partly molten or closed structures
16-10-2015	210	12	350	20 till 21	Squares and partly molten or closed structures
21-10-2015	210	12	350	20	Square+ honeycomb, and molten unordered structures
21-10-2015	210	15	350	22	All structures, lines, square and honeycomb
21-10-2015	210	10	350	10	Dots, squares and some honeycombs
23-10-2015	210	15	350	25	Square and honeycomb also many bad parts on tem grid
23-10-2015	210	20	350	25	Mostly squares also many bad parts on tem grid
23-10-2015	210	15	350	30	Square with molten parts
28-10-2015	220	15	350	22	Mostly molten
28-10-2015	220	17	350	22	Mostly molten
28-10-2015	220	15	350	23	Mostly molten
04-11-2015	220	15	350	18	Mostly molten
04-11-2015	220	17	350	18	Mostly molten, some square

04-11-2015	220	17	350	23	Some square structures
11-11-2015	220	17	350	23	Squares and lots of molten stuff
11-11-2015	660(2hr)	17	1,05mL	23	Squares and lots of molten stuff
13-11-2015	660 (3hr)	17	1,05mL	23	Squares and lots of molten stuff
13-11-2015	220x (+2 petri dishes (pd) with hex under closed cap)	17	350	23	Self-assemblies of dots and small attached structures
19-11-2015	220x (+2 pd with hex under closed cap)	17	350	23	Self-assemblies of dots and small attached structures
20-11-2015	220x (+2 pd with hex under closed cap)	0	350	23	Lines, small squares and molten parts
20-11-2015	220x (+2 pd with hex under closed cap)	17	350	21 at end 10 min @50 C	Lines, small squares and lots of molten parts
24-11-2015	220x (+2 pd with hex under closed cap)	17	350	30	Lines, molten parts and small squares/ honeycombs
24-11-2015	220x (+2 pd with hex open)	17	350	23	More attached square and also honeycombs, but also molten parts
2-12-2015	220x with 2 pd with hex under cap with one hole open	17	350	22	Squares and molten stuff
2-12-2015	220x with 2 pd next to it	17	350	26	Squares and molten stuff

7-12-2015	220x	17	350	22	Square and molten stuff
7-12-2015	220x	17	350	22	Square different patch sizes and molten stuff
11-12-2015	220x	17	350	22	squares
11-12-2015	600x	0	350	22	Lines and squares
23-2-2016	120x(MCT20)	10	350	20	Mostly molten, some small square/ honeycomb part are visible
23-2-2016	120x(MCT20)	5	350	20	Mostly molten, some small square/ honeycomb part are visible
23-2-2016	120x(MCT20)	10	350	22-23	Mostly molten
26-2-2016	120x(MCT20)	12	350	22	Lots of molten structures, some square structures and dots can be seen
26-2-2016	120x(MCT20)	15	350	22	Lots of molten structures, some square structures and dots can be seen
26-2-2016	120x(MCT20)	12	350	22-23	Lots of molten structures, some square structures and dots can be seen